Plasma Chemistry and Plasma Processing, Vol. 23, No. 1, March 2003 (© 2003)

Invited Review

Dielectric-barrier Discharges: Their History, Discharge Physics, and Industrial Applications

Ulrich Kogelschatz[1]

Received April 5, 2002; revised May 7, 2002

Dielectric-barrier discharges (silent discharges) are used on a large industrial scale. They combine the advantages of non-equilibrium plasma properties with the ease of atmospheric-pressure operation. A prominent feature is the simple scalability from small laboratory reactors to large industrial installations with megawatt input powers. Efficient and cost-effective all-solid-state power supplies are available. The preferred frequency range lies between 1 kHz and 10 MHz, the preferred pressure range between 10 kPa and 500 kPa. Industrial applications include ozone generation, pollution control, surface treatment, high power CO_2 lasers, ultraviolet excimer lamps, excimer based mercury-free fluorescent lamps, and flat large-area plasma displays. Depending on the application and the operating conditions the discharge can have pronounced filamentary structure or fairly diffuse appearance. History, discharge physics, and plasma chemistry of dielectric-barrier discharges and their applications are discussed in detail.

KEY WORDS: Dielectric-barrier discharges; silent discharges; non-equilibrium plasmas; ozone synthesis; pollution control; surface treatment; CO_2 lasers; excimer lamps; plasma displays.

1. HISTORY OF DIELECTRIC-BARRIER DISCHARGES

Dielectric-barrier discharges, or simply barrier discharges, have been known for more than a century. First experimental investigations were reported by Siemens[(1)] in 1857. They concentrated on the generation of ozone. This was achieved by subjecting a flow of oxygen or air to the influence of a dielectric-barrier discharge (DBD) maintained in a narrow annular gap between two coaxial glass tubes by an alternating electric field of sufficient amplitude. The novel feature of this discharge apparatus was, that the electrodes were positioned outside the discharge chamber and were not in contact with the plasma (Fig. 1). In his later years Werner von Siemens considered his discharge configuration for the generation of ozone as one of his most important inventions. It is interesting to note, that he never

[1]Retired from ABB Corporate Research, Switzerland.

0272-4324/03/0300-0001/0

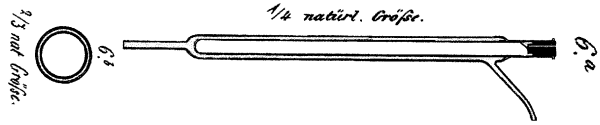

Fig. 1. Historic ozone discharge tube of W. Siemens, 1857 (Ref. 1, *natürl. Grösse* means natural size).

applied for a patent for this configuration, although he received many patents on other subjects. A few years after Siemens' original publication, Andrews and Tait,[2] in 1860, proposed the name "silent discharge," which still is frequently used in the English, German, and French scientific literature (stille Entladung, décharge silentieuse). Ozone and nitrogen oxide formation in DBDs became an important research issue for many decades.[3,4] At the beginning of the 20th century Emil Warburg conducted extensive laboratory investigations on the nature of the silent discharge.[5,6] Becker[7,8] in Germany and Otto[9] in France made important contributions to the design of industrial ozone generators utilizing DBDs. An important step in characterizing the discharge was made by the electrical engineer K. Buss,[10] who found out that breakdown of atmospheric-pressure air between planar parallel electrodes covered by dielectrics always occurs in a large number of tiny short-lived current filaments. He obtained the first photographic traces (Lichtenberg figures) of these microdischarges and oscilloscope recordings of current and voltage. More information about the nature of these current filaments was collected by Klemenc,[11] Suzuki,[12,13] Honda and Naito,[14] and later by Gorbrecht *et al.*[15] and by Bagirov[16] and co-workers. In 1943 T. C. Manley[17] proposed a method for determining the dissipated power in DBDs by using closed voltage/charge Lissajous figures and derived an equation which became known as the power formula for ozonizers. Ozone formation in DBDs was further investigated by Briner and Susz[18] in Switzerland, by Philippov[19] and his group in Russia, by Devins[20] in the United States, by Lunt[21] in England and by Fuji[22] *et al.* in Japan. More recent references can be found in the booklet "Physical Chemistry of the Barrier Discharge" by Samoilovich, Gibalov and Kozlov[23] and in a number of review papers and handbook articles.[24–32] Until about ten years ago, ozone generation was the major industrial application of DBDs with thousands of installed ozone generating facilities used mainly in water treatment. For this reason the dielectric-barrier discharge is sometimes also referred to as the "ozonizer discharge." Occasionally, also the term corona discharge is used in connection with DBDs, although most authors prefer to use this term only for discharges between bare metal electrodes without dielectric. Both discharge types have common features: the generation of "cold" non-equilibrium

plasmas at atmospheric pressure and the strong influence of the local field distortions caused by space charge accumulation. Extensive research activities employing modern diagnostic and modeling tools started around 1970. Originally aimed at a better understanding of the plasma physical and plasma chemical processes in ozonizers, these research efforts resulted not only in improved ozone generators, but also in a number of additional applications of dielectric-barrier discharges: surface modification, plasma chemical vapor deposition, pollution control, excitation of CO_2 lasers and excimer lamps and, most recently, in large-area flat plasma display panels used in wall-hung or ceiling attached television sets. These new applications of DBDs have reached market values substantially larger than the original ozone market. The annual market for plasma displays alone is expected to surpass US$10 billion by the year 2005.

2. THE DIELECTRIC-BARRIER DISCHARGE

Typical planar DBD configurations are sketched in Fig. 2. As a consequence of the presence of at least one dielectric barrier these discharges require alternating voltages for their operation. The dielectric, being an insulator, cannot pass a dc current. Its dielectric constant and thickness, in combination with the time derivative of the applied voltage, dU/dt, determine the amount of displacement current that can be passed through the dielectric(s). To transport current (other than capacitive) in the discharge gap the electric field has to be high enough to cause breakdown in the gas. In most applications the dielectric limits the average current density in the gas space. It thus acts as a ballast which, in the ideal case, does not consume energy. Preferred materials for the dielectric barrier are glass or silica glass, in special cases also ceramic materials, and thin enamel or polymer layers. In some applications additional protective or functional coatings are applied. At very high frequencies the current limitation by the dielectric becomes less effective. For this reason DBDs are normally operated between line frequency and about 10 MHz. When the electric field in the discharge gap is

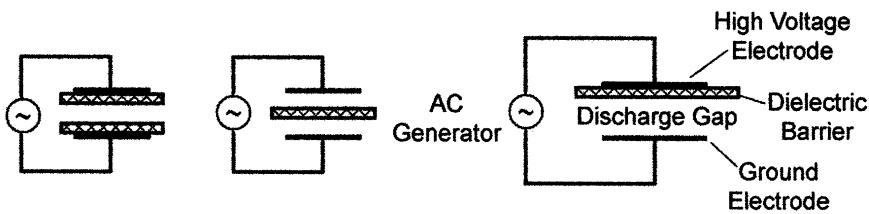

Fig. 2. Basic dielectric-barrier discharge configurations.

high enough to cause breakdown, in most gases a large number of microdischarges are observed when the pressure is of the order of 10^5 Pa. This is a preferred pressure range for ozone generation, excimer formation, as well as for flue gas treatment and pollution control. Figure 3 shows microdischarges in a 1-mm gap containing atmospheric-pressure air, photographed through a transparent electrode.

In this filamentary mode plasma formation resulting in electrical conductivity are restricted to the microdischarges. The gas in between is not ionized and serves as a background reservoir to absorb the energy dissipated in the microdischarges and to collect and transport the long-lived species

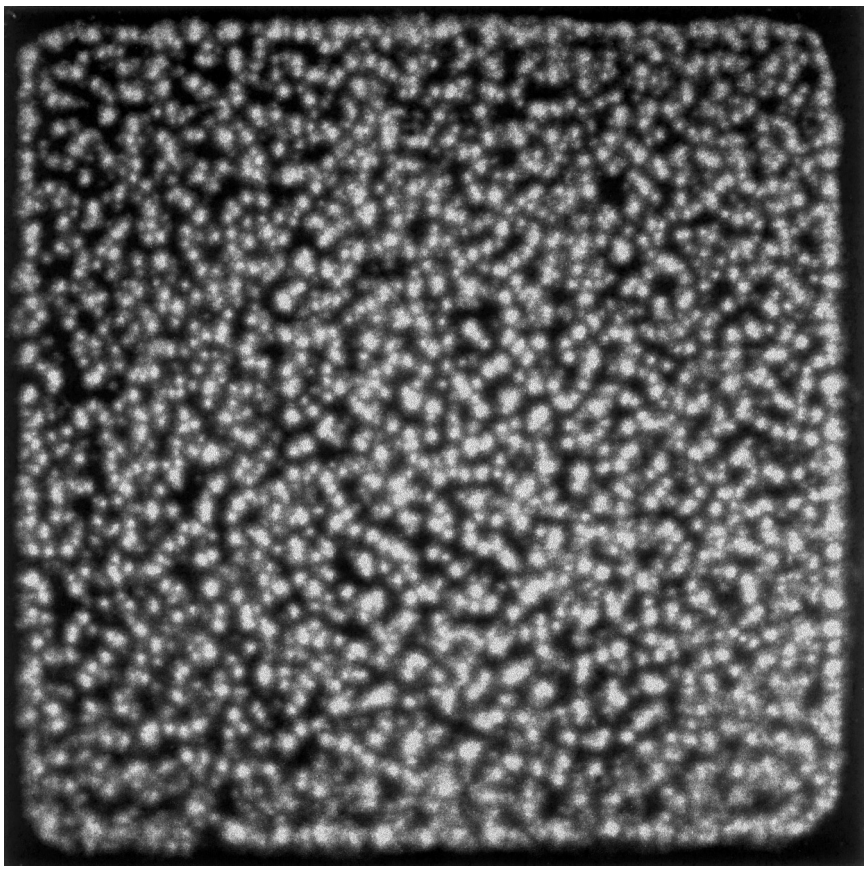

Fig. 3. End-on view of microdischarges in atmospheric-pressure air (original size: 6 cm × 6 cm, exposure time: 20 ms).

created. In most high-power applications liquid cooling of at least one of the electrodes is used.

Besides the planar configuration sketched in Fig. 2 also annular discharge gaps between cylindrical electrodes and dielectrics are used in many technical applications. The discharge gap itself has a typical width ranging from less than 0.1 mm to several centimeters, depending on the application. To initiate a discharge in such a discharge gap filled with a gas at about atmospheric pressure, voltages in the range of a few hundred V to several kV are required. The gas can either flow through the DBD (ozone generation, surface treatment, pollution control) or it can be recirculated (CO_2 lasers) or fully encapsulated (excimer lamps, excimer based fluorescent lamps and light panels, plasma display panels).

2.1. Breakdown Phenomena and Microdischarge Formation

At atmospheric pressure electrical breakdown in a large number of microdischarges is the normal situation for most gases in DBD configurations. Under certain circumstances also apparently homogeneous, diffuse discharges[33–35] can obtained, or also regularly spaced glow discharge patterns.[36–39] Such phenomena are easily obtained in pure He or He-rich gas mixtures or, with special electrode configurations and operating conditions, also in other gases. At lower pressure, typically below 100 Pa, diffuse glow discharges can always be obtained. Such discharges are normally referred to as RF glow discharges and have found widespread applications in the semiconductor industry for plasma etching and plasma deposition processes. These low-pressure discharges have different properties and are not the subject of this article. The most common appearance of dielectric-barrier discharges at elevated pressure, however, is that shown in Fig. 3. It is characterized by a large number of short-lived microdischarges. Each microdischarge has an almost cylindrical plasma channel, typically of about 100 μm radius, and spreads into a larger surface discharge at the dielectric surface(s). Figure 4 shows a schematic diagram of a single microdischarge and a simple equivalent circuit.

By applying an electric field larger than the breakdown field local breakdown in the gap is initiated. In the equivalent circuit that this is symbolized by closing a switch and forcing some of the current through the plasma filament, whose resistance $R(t)$ rapidly changes with time. In reality, growing electron avalanches quickly produce such a high space charge that self-propagating streamers are formed.[25,39–46] A space-charge induced field enhancement at the streamer head, moving much faster than the electron drift velocity, is reflected at the anode and travels back to the cathode where, within a fraction of 1 ns, an extremely thin cathode fall layer is formed. At

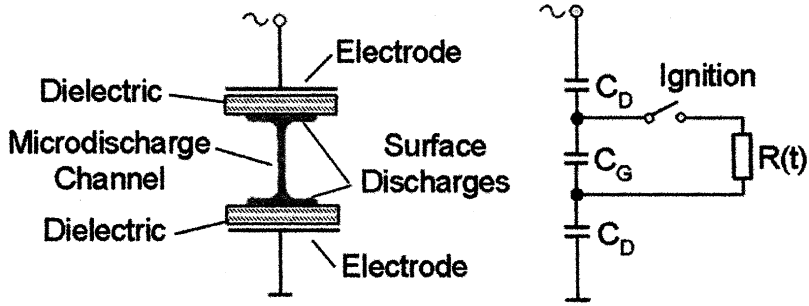

Fig. 4. Sketch of a microdischarge and a simple equivalent circuit.

this moment the current flow through the conductive channel bridging the electrode gap peaks. Subsequently charge accumulation at the dielectric surface(s) reduces the local electric field to such an extent that ionization stops within a few nanoseconds and the microdischarge is choked.

Three stages of microdischarge development are shown in Fig. 5. The metal cathode is at the top, and the anode at the bottom is covered with a dielectric layer ($\varepsilon = 3$, thickness: 0.8 mm). The electron density is shown by

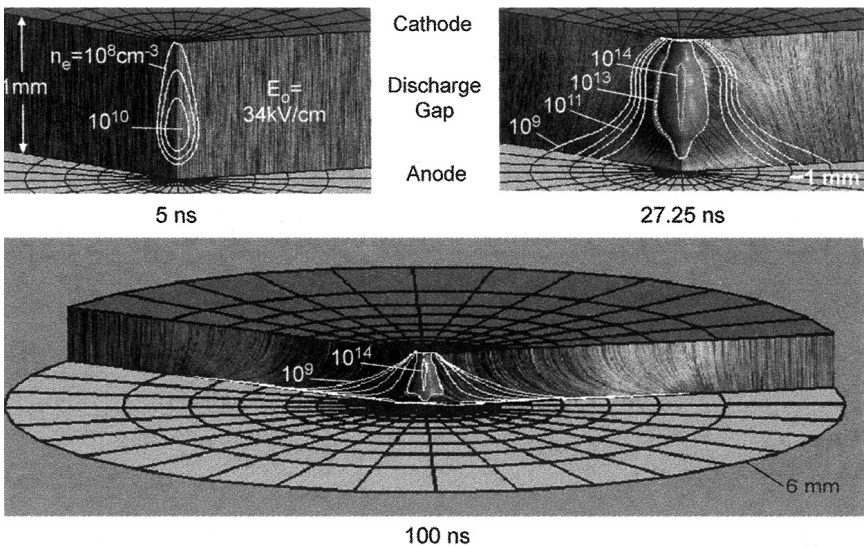

Fig. 5. Two-dimensional numerical simulation of microdischarge development in an atmospheric-pressure mixture of 80% H_2 and 20% CO_2 (computations by W. Egli, Ref. 45).

contour lines. Electric field lines are superimposed. We see the initial electron avalanche travelling towards the anode at 5 ns, the electron distribution at peak current (27.25 ns), coinciding with the formation of the cathode fall region, and a very late stage at 100 ns, long after the current has stopped. At this stage the electrons are still present but the current is choked because the field at this location has collapsed. A few millimeters away from the location of the microdischarge we still find the unperturbed initial homogeneous field of 34 kV/cm. The lateral extension of the surface charge (bottom) is considerably larger than the diameter of the original microdischarge channel. The described choking effect is more pronounced in electronegative gases due to rapid electron attachment.

The plasma filament can be characterized as a transient glow discharge with a developed cathode fall and a positive column. At atmospheric pressure electron densities of 10^{14} to $10^{15}\,cm^{-3}$ and current densities in the range of 100 to $1000\,A\,cm^{-2}$ are reached.[25,41] Surprisingly, computations performed for different gas mixtures always arrive at the same order of magnitude. The cathode layer with extremely high electrical fields extends only about 10 μm into the gap.[42,43,45,46] The described choking effect due to the local field reduction depends on the lateral extension of the surface discharge and the properties of the dielectric barrier and, of course, on the gas properties. For an isolated microdischarge the surface discharge covers an area which is much larger than the channel diameter. The extension of the surface discharge determines the capacitive coupling across the dielectric barrier and the area of reduced field after the termination of the microdischarge. Outside this area of influence we still have undisturbed high-field conditions reached at breakdown (see Fig. 5). As long as the external voltage keeps rising, subsequent microdischarges will therefore preferentially strike at other locations outside this region. Thus, the dielectric serves a dual purpose. It limits the amount of charge and energy imparted to an individual microdischarge and, at the same time, distributes the microdischarges over the entire electrode area. An intact dielectric guarantees that no spark or arc can occur in the discharge gap. Typical charges transported by individual microdischarges are of the order of 100 pC, typical energies are of the order μJ.[25,41,42] As a consequence of the minute energy dissipation in a single microdischarge the local heating effect of the short current pulse is low, in air typically less than 10°C in narrow discharge gaps.

Research on DBDs has focused on tailoring microdischarge characteristics by making use of special gas properties, adjusting pressure and temperature, and optimizing the electrode geometry as well as the properties of the dielectric(s). The radius of a propagating streamer, for example, depends on the gas density n and on the ionization properties of the gas. It is proportional to the reciprocal value of the product of the gas density n and the

derivative of the effective ionization coefficient α_{eff} with respect to the reduced electric field, E/n, taken at breakdown.[25,28] In many gases breakdown occurs at about 100–200 Td (1 Td "Townsend" corresponds to 10^{-17} V cm^2). The effective ionization coefficient α_{eff} is mainly determined by the ionization coefficient α and the attachment coefficient η. In electronegative gases its value practically corresponds to $\alpha_{\text{eff}} = \alpha - \eta$, with a small correction for detachment processes. The slope of α_{eff} vs. E/n at breakdown is much steeper in electronegative gases due to electron attachment. Accordingly, the radii of streamer channels in these gases can be grouped in the following order:

$$\text{oxygen} < \text{carbon dioxide} < \text{air} < \text{nitrogen} < \text{xenon} < \text{helium}.$$

Diffuse discharges can be obtained when, at breakdown, there is sufficient overlap of simultaneously propagating electron avalanches to cause smoothing of transverse field gradients. This condition is met most easily in helium with its relatively wide streamer channels.

The total charge Q transferred in a microdischarge depends on the gas properties and can be influenced by the gap spacing and by the properties of the dielectric. Q is proportional to the width of the discharge gap d, and to the quantity ε/g (ε: relative permittivity, g: thickness of dielectric). The latter relation was experimentally checked to hold up to extreme ε-values of about 1000.[47–49] Contrary to what one might expect, Q does not depend on the gas density.[25]

Recent advances in spectroscopic measuring techniques and in laser diagnostics provided important additional information by *in situ* determinations of electron, atom, free radical and excited species concentrations in individual microdischarges.[50–55] The gas temperature inside microdischarge filaments was derived from rotational band structures.[56–58]

2.2. Microdischarge Plasma Chemistry

The early phases of microdischarge formation are characterized by electron multiplication, by excitation and dissociation processes initiated by energetic electrons, and by ionization processes and space charge accumulation. The ionic and excited atomic and molecular species initiate chemical reactions that finally result in the synthesis of a desired species (e.g., ozone, excimers) or the destruction of pollutants (e.g., volatile organic compounds or VOCs, nerve gases, odours, NH_3, H_2S, NO_x, SO_2, etc.) If the major reaction paths are dominated by charged particle reactions the term plasma chemistry adequately describes the situation. This is the case in many low-pressure discharges. In the majority of DBD applications, however, most charged particles disappear before any major changes occur. In this case it

is most appropriate to speak of a free-radical chemistry primarily involving neutral species like atoms, molecular fragments and excited molecules. In any case, discharge activity and energy dissipation occur mainly within the small volume fraction occupied by microdischarges. The generated active species set the initial conditions for the ensuing chemical reactions. An adequate picture of the physical processes during breakdown and microdischarge formation is prerequisite for a detailed understanding of DBD chemistry. Each individual microdischarge can be regarded as a miniature plasma chemical reactor. Scaling up or increasing the power density just means that more microdischarges are initiated per unit of time and per unit of electrode area. In principle, individual microdischarge properties are not altered during up-scaling.

Typically, the first step is a dissociation of the initially molecular species by electron collisions. Electron impact dissociation of O_2 and N_2[59–66] has been investigated in connection with ozone generation from oxygen and from air. The properties of CO_2[67–70] have, for example, been studied with the aim of optimizing CO_2 lasers. One important question influencing the efficiency of DBD applications is the efficiency of the initial dissociation process with respect to energy consumption. It depends on the fractional energy losses of the different electron collision processes involved. The dissociation of oxygen by electron impact can be highly efficient (up to 85% of the electron energy can be utilized for the dissociation process), provided that the reduced electric field is in the range of 100–300 Td, corresponding to average electron energies of about 4 to 8 eV. This situation is unique in oxygen. In pure nitrogen the fraction of discharge energy spent on dissociation is much less due to energy lost for the excitation of vibrational levels. In CO_2 under favourable conditions, at most 40% of the electron energy can be utilized for the dissociation process. The efficiency of the different processes involved depends on their cross sections for electron collisions and the reduced field E/n.

2.3. Numerical Modeling

Depending on the goal different modeling approaches have been taken. To clarify the dynamics and kinetics of chemical changes rather extensive reaction systems including free radical reactions have been treated. Since the dominant reactions are fast, as a first step, this may be carried out neglecting spatial variations. To simulate effects of re-striking microdischarges it is useful to investigate repetitive injection of electrons or free radicals.[28,71–74] In many cases the final products depend in a complex way on the assumed repetition rate and on intermediate concentrations of transient species.

To model the formation of a microdischarge 2D models are required. Early phases can be treated with equations also used to describe streamer propagation in pulsed corona discharges. To include the choking action of the dielectric barrier(s) introduction of additional boundary conditions is required, which can treat charge accumulation at the dielectric surface and the resulting local reduction of the electric field in the discharge gap. As soon as the field falls below the value necessary to sustain ionization the microdischarge decays. Clearly, this process is faster in gas mixtures showing strong attachment.

For the 2D simulations of microdischarge development shown in Fig. 5 rotational symmetry was assumed. Two equation sets were used to describe the evolution of a microdischarge. The continuity equations for the charged species n_i (electrons, positive and negative ions) with source and sink terms S_i (describing ionization and attachment) can be written as

$$\frac{\partial n_i}{\partial t} + \nabla \cdot (v n_i + D_i \nabla n_i) = S_i \tag{1}$$

where $v = \mu E$ is the drift velocity, defined as mobility μ times electric field strength E and D_i is the diffusion coefficient. E again is defined as the gradient of the potential ϕ, $E = -\nabla\phi$. It is related to the charge density ρ by Poisson's equation

$$\nabla^2 \phi = -\frac{\rho}{\varepsilon} \tag{2}$$

The equations have to be solved simultaneously in the discharge gap and inside the dielectric with appropriate boundary conditions at the interface. Fast Poisson solvers and special grids were used to keep computation times within reasonable limits.

To consider also the radial expansion of the microdischarge channel during chemical changes rather complex 2D models treating breakdown, plasma chemistry and hydrodynamic expansion have been developed.[74,75] Also the interaction of adjacent microdischarges has been attacked.[76] Rather sophisticated numerical models have recently been developed to describe discharge initiation, excitation and the generation of VUV radiation in rare gas mixtures used in miniature plasma display pixel cells.[77–82]

At atmospheric pressure collision rates are high and electrons reach equilibrium conditions corresponding to the local field within picoseconds. Microdischarges develop at a nanosecond time scale, free radical reactions may take microseconds to milliseconds, and ground state chemical reactions may take much longer to reach equilibrium conditions. The rate coefficients for electronic collisions primarily depend on the reduced electric field E/n

or the mean electron energy. Rate coefficients for chemical reactions may strongly depend on the gas temperature. The use of tabulated values for the rate coefficients of electron-induced reactions is justified if steady state conditions are reached faster than the relevant changes occur and if electric field gradients are not too steep. The validity of this "local field approximation" can be checked by Monte Carlo calculations of individual electron paths. From such calculations we know that in atmospheric-pressure gases electrons approach steady state values in about 20 ps.[83] This is roughly one thousand times shorter than the typical duration of a microdischarge.[41]

2.4. Overall Discharge Parameters

Since microdischarge development occurs at a nanosecond time scale and the operating cycle in most applications is of much longer duration, DBDs are normally characterized by a large number of microdischarges per unit of electrode area and per cycle. A typical value is about 10^6 microdischarges per cm^2 per second.[84] This number depends primarily on the power density. It is also influenced by the presence of UV radiation. For a given configuration and fixed operating parameters all microdischarges are of similar nature. They are initiated at a well-defined breakdown voltage, and they are terminated after a well-defined current flow or charge transfer. For many purposes it is sufficient to describe the discharge by overall quantities: the applied frequency f, the maximum applied voltage $\hat{U}$ and the average discharge voltage U_{Dis} in the gap, at which microdischarge activity is observed. The interesting feature of the DBD power formula first proposed by Manley[17] is, that only the peak value of the applied voltage enters and not its form.

$$P = 4 f C_{\mathrm{D}} U_{\mathrm{Dis}} \{ \hat{U} - C_{\mathrm{D}}^{-1} (C_{\mathrm{D}} + C_{\mathrm{G}}) U_{\mathrm{Dis}} \}, \qquad \hat{U} \geq C_{\mathrm{D}}^{-1} (C_{\mathrm{D}} + C_{\mathrm{G}}) U_{\mathrm{Dis}} \quad (3)$$

It relates the total power P to the operating frequency f, the peak voltage $\hat{U}$ and the capacitances of the dielectric(s) (C_{D}) and the discharge gap (C_{G}), quantities that characterize the electrode configuration. Since the (fictitious) average discharge voltage U_{Dis} cannot be determined directly it is sometimes more convenient to use the quantity U_{Min} instead, the minimum external voltage at which microdischarges are observed in the discharge gap.

$$P = 4 f C_{\mathrm{D}}^2 + (C_{\mathrm{D}} C_{\mathrm{G}})^{-1} U_{\mathrm{Min}} (\hat{U} - U_{\mathrm{Min}}), \qquad \hat{U} \geq U_{\mathrm{Min}} \quad (4)$$

The simple relation $U_{\mathrm{Min}} = (C_{\mathrm{D}} + C_{\mathrm{G}}) C_{\mathrm{D}}^{-1} U_{\mathrm{Dis}}$ connects these quantities. As a matter of fact, this relation can be used as a definition of U_{Dis}. The power formula has proved very useful for a large variety of dielectric-barrier discharges. It is used in many technical developments. For a given configuration and fixed peak voltage the power is directly proportional to the

frequency. The reason is that we generate the same number of identical microdischarges per period. The discharge voltage depends on nature of the gas mixture, the gas density and the width of the discharge gap. Microdischarge activity, symbolically indicated in Fig. 6 by short peaks on top of the capacitive current, is observed only when the voltage in the gap reaches U_{Dis}. During these phases ($2 \rightarrow 3$ and $4 \rightarrow 1$) the slope in the Lassajous figure corresponds to the capacitance of the dielectric(s). During the rest of the cycle it corresponds to that of the electrode configuration in the absence of a plasma.[85] Depending on the peak voltage microdischarge activity is limited to a certain fraction of the cycle and occurs at twice the driving frequency.

The experimental determination of the power dissipated in DBDs has often proved to be difficult because in reality the power is consumed in a large number of short-lived microdischarges. Following the original work of Manley many authors have used voltage/charge Lissajous figures to determine the average power. The trick is to use the time-integrated current, the charge, rather than trying to resolve individual microdischarge current peaks. This can be achieved in a simple way by putting a capacitance in series with the DBD experiment.[85] The voltage across this measuring capacitor is proportional to the charge. It can be rigorously shown that the area of a closed loop of the applied voltage vs. charge always represents the energy consumed during one period.[17,85,86]

The form of this voltage/charge Lissajous figure contains important information about the discharge. For an ideal capacitance the Lissajous figure collapses into a straight line, a resistive load results in an ellipse. In the majority of DBD applications (ozone generators, excimer lamps) the figure is close to an ideal parallelogram, from which the discharge voltage and the effective capacitances of the discharge gap and the dielectric(s) can

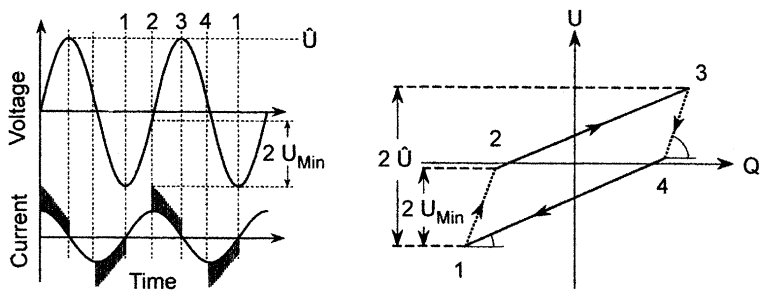

Fig. 6. Symbolic presentation of microdischarge activity and corresponding voltage/charge Lissajous figure.

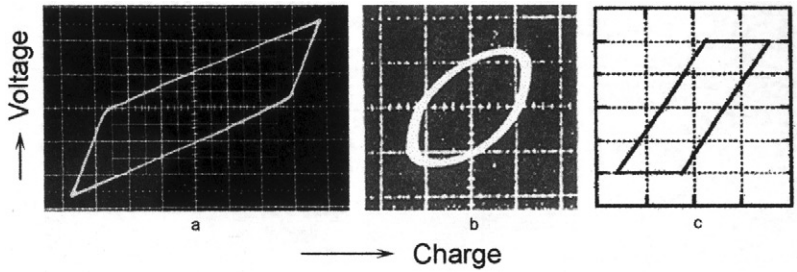

Fig. 7. Voltage/charge Lissajous figures of different dielectric-barrier discharge types. (a) ozone tube at 1 kHz, (b) CO_2 laser at 50 kHz, (c) plasma display at 100 kHz square wave voltage, Refs. 85, 242, 87).

be inferred (see Fig. 7). In the case of silent-discharge CO_2 lasers (4 cm discharge gap at 13 kPa) the Lissajous figure resembles an ellipse, indicating the presence of residual ions at all times. In the case of a plasma display cell operated with a 100-kHz square wave voltage the figure is again a parallelogram with two almost horizontal sections.[87] Also, plots of current vs. voltage are used to obtain information about ignition and decay of the discharge.

3. OZONE GENERATION

After Christian Friedrich Schönbein,[88] in 1839, had identified ozone as a new chemical compound, Werner Siemens, in 1857, proposed his method for reliably generating ozone by passing air or oxygen through an ac discharge bounded by at least one dielectric barrier.[1] Both gases, oxygen or air, are still used today for industrial ozone generation, preferably at pressures 0.1 and 0.3 MPa. As mentioned before, in oxygen or air at atmospheric pressure or above, the discharge is of filamentary nature. The number of microdischarges per unit of electrode area and time depends on the power density. Their strength (energy-density, transferred charge), is determined by the gap spacing, pressure and dielectric properties.

3.1. Reaction Kinetics of Ozone Formation from Oxygen and from Air

The control of the plasma conditions inside the microdischarge columns is of eminent importance for optimizing the reaction kinetics of ozone formation.[23–32,40–44,85,89–92] For a given feed gas composition and desired power density this can be achieved by adjusting the operating parameters pressure, and/or gap width as well as the properties of the dielectric barrier

(permittivity, thickness), and the feeding circuit. The plasma conditions in the microdischarges have to be optimized for exciting and dissociating oxygen and nitrogen molecules. Initially, the major fraction of the energy gained by the electrons in the electric field is deposited in excited atomic and molecular states. Starting from electron impact on ground state O_2 molecules two reaction paths leading to dissociation are available: via excitation of the $A\,^3\Sigma_u^+$ state with an energy threshold of about 6 eV and via excitation of the $B\,^3\Sigma_u^-$ state starting at 8.4 eV. Ozone is then formed in a three-body reaction, involving O and O_2, leading to the formation of the O_3 molecule.

$$O + O_2 + M \rightarrow O_3^* + M \rightarrow O_3 + M \tag{5}$$

M is a third collision partner: O_2, O_3, O or, in the case of air, also N_2. O_3^* stands for a transient excited state in which the ozone molecule is initially formed after the reaction of an O atom with an O_2 molecule. The time scale for ozone formation in atmospheric pressure oxygen is a few microseconds. Side reactions, also using O atoms, compete with ozone formation.

$$O + O + M \rightarrow O_2 + M \tag{6}$$

$$O + O_3 + M \rightarrow 2O_2 + M \tag{7}$$

$$O + O_3^* + M \rightarrow 2O_2 + M \tag{8}$$

The undesired side reactions (6)–(8) pose an upper limit on the atoms concentration, or the degree of dissociation, tolerable in the microdischarges. Optimizing microdischarge properties for the ozone formation process amounts to finding a compromise between excessive energy losses due to ions in weak microdischarges and avoiding undesired chemical side reactions when the microdischarges become too strong. Model calculations using many additional reactions in oxygen suggest a reasonable compromise at relative atom concentrations of the order 0.2% in a microdischarge channel.[41]

In air discharges the presence of the nitrogen ions N^+, N_2^+, nitrogen atoms and excited atomic and molecular species add to the complexity of the reaction system.[42–44,61,93–98] For mixtures of 20% oxygen and 80% nitrogen, simulating dry air, and also in humid air the chemical changes due to a short discharge pulse were computed using fairly extended reaction schemes.[99,100] In addition to ozone a variety of nitrogen oxide species are generated: NO, N_2O, NO_2, NO_3, and N_2O_5, all of which have been detected by spectroscopic techniques[75,95,101,102] or by dynamic mass spectrometry.[103] The main aspects of ozone generation in dry air can be summarized as follows. Excitation and dissociation of nitrogen molecules lead to a number

of additional reaction paths involving nitrogen atoms and the excited molecular states $N_2(A\,^3\Sigma_u^+)$ and $N_2(B\,^3\Pi_g)$ that can produce additional oxygen atoms for ozone generation.

$$N + O_2 \rightarrow NO + O \tag{9}$$

$$N + NO \rightarrow N_2 + O \tag{10}$$

$$N_2(A) + O_2 \rightarrow N_2O + O \tag{11}$$

$$N_2(A, B) + O_2 \rightarrow N_2 + 2O \tag{12}$$

About half of the ozone formed in air discharges results from these indirect processes.[42,61] As a a result, ozone formation in air takes longer (about 100 μs) than in oxygen (about 10 μs), and a substantial fraction of the electron energy initially lost in collisions with nitrogen molecules can be recovered and utilized through reactions (9)–(12) for ozone generation.

At a certain level of NO/NO_2 concentrations, which can easily be reached in ozone generators by reducing the air flow or by applying excessive power, ozone formation breaks down completely. This state is referred to as discharge poisoning, a phenomenon already observed by Andrews and Tait[2] in 1860. Under such conditions neither ozone nor N_2O_5 appears in the product gas. Instead, NO, NO_2, and N_2O are detected. This state is characterized by rapid NO_x reactions, consuming oxygen atoms at a faster rate than the ozone formation reaction (5). The result is an accelerated recombination of oxygen atoms, catalyzed by the presence of NO and NO_2. Previously formed ozone is removed in a catalytic ozone destruction process also involving NO and NO_2.[27]

According to Crutzen[104] and Johnston[105] similar reactions also influence the stratospheric ozone concentration. Reactions involving NO and NO_2 are extremely fast so that relatively small NO_x concentrations on the order of 0.1% can seriously interfere with ozone formation. These effects can readily be demonstrated in ozone generators. If traces of NO or NO_2 are added to the feed gas oxygen or air at the intake of an ozone generator ozone formation is inhibited. Elevated temperature in the discharge gap can be another reason for reduced ozone generation or complete absence of ozone at the exit. As Schultz and Wulf[106] demonstrated in 1940 an air-fed ozonizer operated at the high temperature of 800°C produces mainly nitrogen oxides.

3.2. Technical Aspects of Industrial Ozone Generation

The first major ozone installations in drinking water plants using ozone for disinfection were built around the beginning of the last century in Paris

(1897) and Nice (1904), France, and in St. Petersburg, Russia (1910). Dielectric plates or tubular dielectrics in the form of glass tubes were used. More recently, industrial ozone generation has profited substantially from a better understanding of the ozone formation process in dielectric-barrier discharges including ways of tailoring microdischarge properties.[107,108] Also, the replacement of line frequency and low frequency motor-generator sets by static frequency converters using modern power electronics led to important innovations in the power supply units and in process control. The use of higher frequencies brought the advantage of lower operating voltages for a given input power. This resulted in reduced strain on the dielectrics. In addition the power densities were increased substantially. As a result, higher ozone production rates and much higher ozone concentrations are reliably attained in much more compact ozone generators.[85,107,108] In this context it may be of interest to point out, that already in 1921 Starke[109] had demonstrated that the energy efficiency of the ozone formation process does not depend on the applied frequency between 50 Hz and 10 kHz.

Most technical ozone generators use cylindrical discharge tubes of about 20–50 mm diameter and 1–3 m length. The favorite dielectric material has for a long time been borosilicate glass. In many technical ozone generators Pyrex (Duran) glass tubes, closed at one side, are mounted inside slightly wider stainless steel tubes to form annular discharge gaps of about 0.5–1 mm radial width (see Fig. 8). Geometrical tolerances of steel and glass tubes as well as mounting procedures for the glass tubes have been important issues in technical ozone generators. Local deviations from the design gap width have an important influence on microdischarge properties, on the mass flow, the power deposition and on the heat flow to the cooled steel

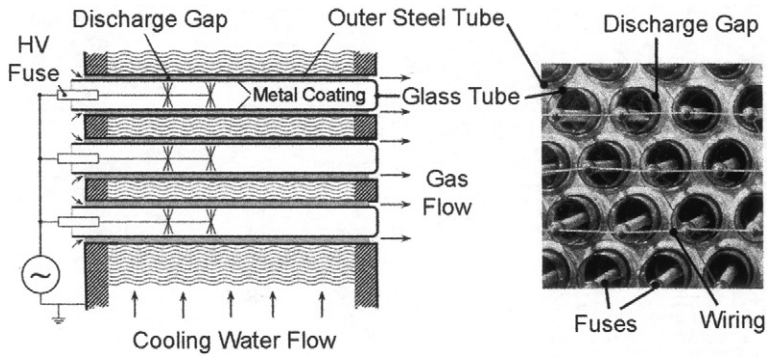

Fig. 8. Configuration of discharge tubes in a technical ozone generator (not to scale).

electrode. Such deviations can result in drastic reductions of the ozone generating efficiency. Superior performance has been obtained with precise, extremely narrow discharge gaps of 0.1 mm width.[110]

Metal coatings, e.g., thin aluminum films, inside the glass tubes serve as high-voltage electrodes, which are contacted by metal brushes. Modern high-performance ozone generators use non-glass dielectrics in the form of thin coatings on steel tubes. Typically, a number of layers with optimized dielectric characteristics are deposited. These coated steel tubes are less fragile than the traditional Pyrex tubes. Individual discharge tubes are protected by high-voltage fuses (Fig. 8). In case of dielectric failure the fuse blows and disconnects the faulty element. This way, the other tubes can stay in operation. Large ozone generators use several hundred, actually close to one thousand, discharge tubes inside big steel tanks to provide the required electrode area for mass ozone production. The outer steel tubes are welded to two paraallel end flanges thus forming a sealed cooling compartment in a conventional heat exchanger configuration. They are cooled by a transverse water flow. Efficient cooling is essential for good performance because the ozone forming reaction and also the low thermal stability of the ozone molecule demand low operating temperatures. The design of the cooling water flow requires major attention. Since the gas flow close to the exit of the discharge tubes contains the highest ozone concentrations this section is most sensitive to high temperatures. The inlet part of the tubes with low ozone concentrations is much less sensitive to temperature. Therefore, the cooling water flow has to be designed in such a way that the incoming cold water first cools the exit section of discharge tubes. It is essential to avoid re-circulating regions in the water flowing through the tank.

An alternative technology mainly employed in small ozone generators is the use of surface discharges with thin parallel electrode strips deposited on ceramic tubes. This electrode configuration was originally proposed by the late S. Masuda[111] and co-workers in 1988. It had only a minor impact on mass ozone production, but it is used to a large extent, in a slightly modified version, in plasma displays today.

Modern high-power ozone generators utilize advanced semiconductor power conditioning. They make use of thyristor- or transistor-controlled frequency converters to impress square-wave currents or specially formed pulse trains in the medium frequency range. Typical fundamental operating frequencies are between 0.5 and 5 kHz. Using this technology, applied voltages have been reduced to the range of about 5 kV, thus practically eliminating the risk of dielectric failure. With large ozone generators power factor compensation has become an important issue. Typical power densities now reach 1–10 kW/m^2 of electrode area. Large ozone installations reach input

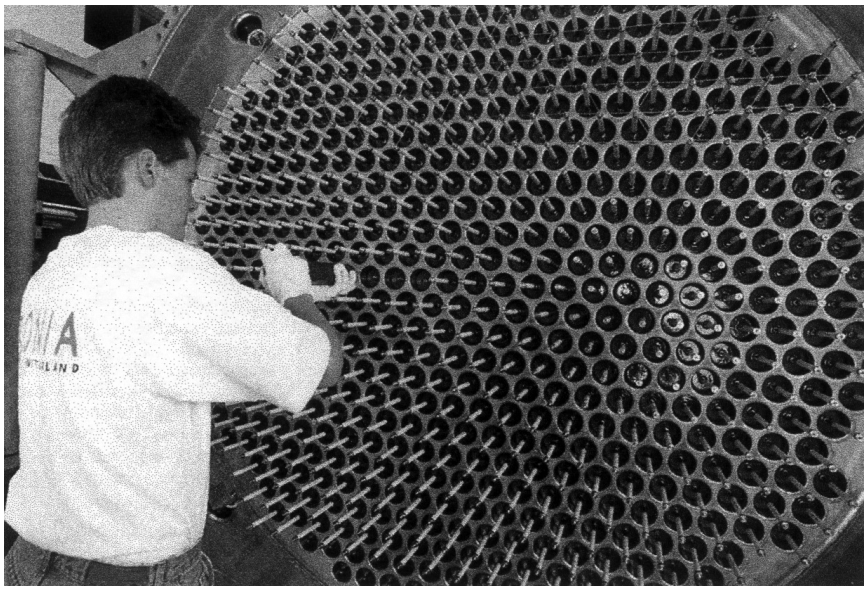

Fig. 9. Advanced ozone generator producing 60 kg/h with non-glass dielectrics (Ozonia Ltd.)

powers of several MW. The ozone generating capacity of one big tank is now in the range of 100 kg/hr.

Ozone concentrations up to 5% (wt) from air and up to 18% can be reached using oxygen feed. Modern water works utilize ozone at concentrations up to 12%. Considerable progress has been made in recent years with respect to attainable ozone concentrations and energy consumption. Ozone properties, ozone applications, and ozone technologies were reviewed in detail by Wojtowicz,[112] the ozone chemistry in water was treated by Hoigné.[113]

3.3. Feed Gas Preparation

Ozone generators are normally operated with dried clean air or dry oxygen. In both cases the dew point should be kept below –60°C. This limits the water vapor content to a few ppm. Humidity in the feed gas has two adverse effects on ozone generation. It increases the surface conductivity of the dielectric resulting in stronger microdischarges. Through the formation of OH and HO_2 radicals it also interferes with the ozone formation reactions by introducing additional catalytic ozone destruction mechanisms. In the presence of OH radicals NO and NO_2 molecules are rapidly converted to

HNO_2 and HNO_3, respectively. Negative effects on the ozone formation efficiency are also observed when traces of H_2 or hydrocarbons are present in the feed gas. Both impurities have an adverse influence on ozone generation.[108,114,115] Most large ozone generators use pure oxygen or oxyen blended with about 1% nitrogen as a feed gas. The presence of nitrogen has a pronounced beneficial effect on ozone generation. Especially at high specific energies, traces of nitrogen increase the ozone production efficiency and the attainable ozone concentration compared to the values obtained in pure oxygen.[108]

4. DEPOLLUTION OF GAS STREAMS

Since dielectric-barrier discharges, based on the mature ozone-generation technology, can operate at high power levels and can treat large atmospheric-pressure gas flows with negligible pressure drop, potential applications in pollution control have been systematically examined.[26–30,32,116–125] The utilization of dielectric-barrier discharges for the control of gaseous pollutants and the destruction of poisonous compounds has been addressed by several researchers. Early investigations on the destruction of H_2S were carried out by Berthelot[126] in 1876 and by Schwarz and Kunzer in 1929.[127] The subject was taken up again by Traus and Suhr[128] in 1992. Some work on military toxic wastes was carried out by Clothiaux *et al.*[129] and by Fraser and Sheinson.[130] Much work has been devoted to the decomposition of nitrogen oxides and sulphur oxides in flue gases[131–134] and of volatile organic compounds (VOCs), such as hydrocarbons, chlorocarbons and chlorofluorocarbons (CFCs), perfluorocarbons (PFCs), and other hazardous air pollutants (HAPs). Contamination of exhaust air with VOCs occurs in many industrial processes, e.g., in semiconductor manufacturing, in chemical processing, in dry cleaners, and in print and paint shops. VOC contamination of soils and water can often be treated in the gas phase after vapor extraction of the VOCs.[119] Odour control in animal houses and fish factories is still another application of dielectric-barrier discharges. In many cases the treatment involves the destruction of H_2S and NH_3.[128,135–138]

4.1. Principles of Non-Thermal Plasma Remediation of Gaseous Pollutants

Many hazardous organic molecules are readily attacked by free radicals, electrons, or UV photons. In many cases the carrier gas is air. Dielectric-barrier discharges are used to provide reactive species such as $N_2^*(A\,^3\Sigma_u^+)$, $N_2^*(B\,^3\Pi_g)$, $O_2^*(a^1\Delta_g)$, $O(^1D)$, $O(^3P)$, and $N(^4S)$. In exhaust and flue gases water vapor may play an important role. In addition to direct dissociation

of water molecules by electrons, species initially formed by electron collisions in the microdischarge filaments, subsequently react with H_2O to form additional H, OH, or HO_2 radicals for decomposing pollutants.

$$N_2^* + H_2O \rightarrow OH + H + N_2 \tag{13}$$

$$O(^1D) + H_2O \rightarrow OH + OH \tag{14}$$

$$O_3 + OH \rightarrow HO_2 + O_2 \tag{15}$$

$$H + O_2 + M \rightarrow HO_2 + M \tag{16}$$

DBDs are normally run at conditions in which radical concentrations in optimized microdischarges are so low that radical–radical recombination or annihilation reactions between radicals can be neglected. The hydroxyl radical (OH) is an extremely efficient oxidant, with an oxidizing potential (2.8 V) substantially higher than that of ozone (2.07 V). It is the dominant oxidant in many applications, which also plays an eminent role in cleaning the troposphere.[139] In industrial pollution control applications the aim is to convert toxic compounds to form non-hazardous or less hazardous substances such as O_2, O_3, CO, CO_2, H_2O, simple acids or, upon addition of ammonia, to form solid salt particles, that can easily be disposed of, or can be used as fertilizers. In some applications additional selective catalytic converters and dust collection devices follow the plasma treatment.

4.2. Treatment of Volatile Organic Compounds

As far as DBD plasma remediation is concerned several successful laboratory and pilot investigations have been reported in the literature.The destruction of methane (CH_4),[140] butane (C_4H_{10}),[141] propene (C_3H_6),[142] benzene (C_6H_6),[143–145] toluene (methylbenzene, $C_6H_5CH_3$),[119,146,147] styrene (vinylbenzene, $C_6H_5CHCH_2$),[148] xylene (dimethylbenzene, $C_6H_4(CH_3)_2$),[147,149] formaldehyde (HCHO),[145,150] acetaldehyde (CH_3CHO),[151] methanol (CH_3OH),[120,152] propanol (C_3H_7OH)[153] carbon tetrachloride (CCl_4),[117,119–121,153–155] dichloromethane,[156] trichloroethane (TCA, $C_2H_3Cl_3$),[119,121] trichloroethylene (TCE, $ClHC{=}CCl_2$),[117,119,121,147,152–155,157–159] perchloroethylene (PCE, C_2Cl_4),[72,119,160] methylene chloride (CH_2Cl_2),[120] chlorobenzene (C_6H_5Cl),[161] and tetrafluoromethane (CF_4),[162] was investigated.

In general it can be stated that non-equilibrium plasmas use most of the discharge energy to produce and accelerate electrons. The electrons then generate highly reactive free radicals which can selectively decompose toxic compounds. This can be achieved at low gas temperatures and at atmospheric pressure, conditions that are of utmost importance for flue gas or

off gas treatment. At dilute pollutant concentrations, typically less than 1000 ppm, non-equilibrium plasma treatment requires substantially less energy than incineration or thermal-plasma treatment. In many cases it is also more economical than raising the temperature of the entire gas flow to temperatures where catalytic decomposition can be achieved (200–500°C). In many laboratory investigations dielectric-barrier discharges achieve similar results to those obtained in pulsed corona discharges or with electron beam injection. The main advantage of DBDs is their simplicity and the availability of reliable, efficient and affordable power supplies. Compared to pulsed corona discharges they require no sophisticated pulsing circuits and compared to electron beam treatment they require no vacuum chambers with delicate windows separating the acceleration chamber from the polluted atmospheric-pressure environment. Even more important, contrary to most other discharges, dielectric-barrier discharges can be scaled up without additional difficulties.

Following the work of Foster and Butt[163] in 1972 a large number of investigations have used pellets with different dielectric and catalytic properties inside the discharge gap of dielectric-barrier discharges[164–166] (see also Refs. 135, 138, 140, 141, 143, 144, 147, 151, 153, 155, and 156). Such pellets have a strong influence on the discharge, which is now forced to ignite in the interstices between pellets and on their surfaces. Special pellet materials and coatings lead to additional catalytic processes. A more recent suggestion is to ignite barrier discharges inside the pores of reticulated ceramic foams,[167] which also may have additional catalytic coatings to promote the desired reactions.

4.3. Treatment of Diesel Exhaust Gases

The treatment of NO_x in Diesel exhaust streams of passenger vehicles and trucks has recently become an important issue with potentially large markets for dielectric-barrier discharges.[168–170] Modern direct-injection Diesel engines offer a fuel economy unmatched by any other automotive engines. For this reason major automobile companies are investigating Diesel engines to meet the CO_2 emission reductions required by the Kyoto Protocol. Using Diesel engines on a large scale would require better NO_x and particulate control of the exhaust streams. Initial experiments showed that the reduction of NO in N_2 carrier streams is feasible.[171] In a real Diesel exhaust stream, however, the presence of oxygen and water vapor leads to a highly oxidizing environment under plasma conditions. As a consequence, desired reductive reaction paths converting NO to N_2 and O_2 are only of minor importance. Recent experiments show that with the aid of hydrocarbon additives (unburned fuel) a selective oxidation of NO to NO_2 is

possible without the undesired formation SO_3 from SO_2. Also the formation of HNO_2 and HNO_3 can be suppressed, even in the presence of water vapor. The presence of some hydrocarbons, like ethene, propene, and propane, dramatically changes the reaction kinetics of NO oxidation. In such a plasma environment HO_2 and peroxy radicals (R–OO) are the dominant oxidants (R–OO=H_3C–CH(OO)–CH_3, H_3C–CH_2–CH_2(OO), or HOC_2H_4OO).

$$NO + HO_2 \rightarrow NO_2 + OH \tag{17}$$

$$NO + R\text{–}OO \rightarrow NO_2 + R\text{–}O \tag{18}$$

HO_2 is produced from a reaction of H with O_2, the peroxy radical from reactions of hydroxyalcyl and alcyl radicals, which also quickly react with O_2. Measurements as well as numerical simulations show that the energy required to oxidize an NO molecule can be substantially reduced in the presence of ethene,[172,173] and propene, or propane.[73,170,172,174]

The most promising scheme for Diesel exhaust treatment is a hybrid system using DBD plasma oxidation followed by a heterogeneous process that can chemically reduce NO_2 to N_2, O_2, and H_2O by selective catalysis.[168,17,0,175] This process is referred to as plasma enhanced selective catalytic reduction (PE–SCR). Extensive modeling efforts have been devoted to the plasma kinetics of NO_x in dry and wet air streams[94–96,101,176–183] and to the role of unburned hydrocarbons (UHCs)[170,171,184,185] and particles (soot)[186] in exhaust streams. For more detailed information the reader is referred to the PhD theses of M. Klein,[187] S. Bröer[188] and the MS thesis of R. Dorai.[189] DBD plasmas can also be used to eliminate submicron size soot particles formed during fuel combustion.[190]

4.4. Gas Liquefaction and Greenhouse Gas Abatement

Early investigations aimed at the cracking of hydrocarbons in DBDs date back to de Saint-Auney[191] in 1933. They were followed by investigations of Zhitnev and Philippov[192] in 1967 and those by Rutkowsky[193] *et al.* in 1982. The mechanism of hydrocarbon decomposition in electrical discharges was discussed by Slovetsky.[194] More recently the subject has attracted much attention in the context of converting natural gas or hydrogen to a liquid fuel and coping with greenhouse gas emissions.[195] There is a considerable interest in converting off-shore methane to middle distillates. Different groups investigate the hydrogenation of CO_2 and the partial oxidation of CH_4 in DBDs.[28,71,196–202] Methanol formation has been observed in CH_4/O_2 mixtures and in CH_4/air mixtures.[203,204] Methanol, a liquid at standard conditions, can be handled like gasoline and can be used in a

conventional car engine or, in connection with a reformer, to power a fuel cell driving an electric motor. The difficulties met in storing, transporting, and distributing hydrogen can be avoided when a liquid fuel is used instead.

High conversion rates of more than 60% have been obtained in DBDs running on CO_2/CH_4 mixtures, the two most abundant greenhouse gases.[205,206] The main product is syngas, a mixture of CO and H_2, which is considered a valuable feedstock for many chemical processes, including methanol synthesis. So far these investigations have mainly been of academic interest, because the discharge energy is still too high to meet economic requirements. Further improvements are expected from a better understanding of the plasma kinetics, better discharge control, and the simultaneous use of catalysts.[207]

5. SURFACE TREATMENT

With the advent of readily available and affordable plastic foils and other polymer materials about 1960 it soon became apparent that, for a number of applications, their surface properties required modification. Most plastics have non-polar chemically inert surfaces making them non-receptive to bonding, to printing inks, coatings, and adhesives. The main property responsible for this behavior is the low surface energy. One possibility to substantially increase the surface energy of different substrates is corona treatment in atmospheric-pressure air. It developed into a reliable surface treatment process that can match the production speed of foils.[208–210] The term corona treatment stems from the early days when thin wires, threaded-rod, or knife-edge electrodes where used as corona electrodes. In the meantime most commercial "corona treaters" in fact employ dielectric-barrier discharges by covering the rotating drum or the electrodes with dielectrics. Figure 10 shows a sketch of a modern version using water-cooled ceramic tube electrodes.[211]

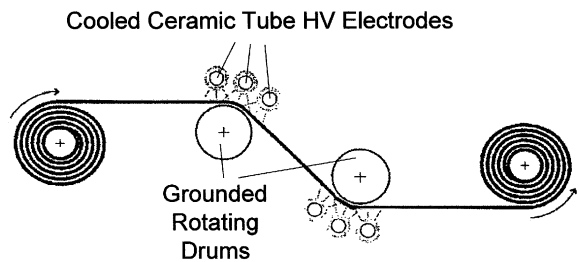

Fig. 10. Continuous double-sided foil treatment with dielectric-barrier discharges (after Ref. 211).

The use of DBDs has the advantage that the presence of the dielectric prevents electric puncture of the plastic foils in case of pinholes and that also electrically conductive webs and metallic foils can be treated. Large corona treaters handle foils up to 10 m width at speeds surpassing 10 m/s. Operating with discharge gaps of a few millimeters width in atmospheric-pressure air leads to the filamentary silent discharge known from air-fed ozone generators (Fig. 3). Typical operating frequencies are in the range 10–50 kHz, generated by solid-state power supplies now reaching output powers of more than 50 kW. The development of HV power devices like SCRs (silicon controlled rectifiers or thyristors) and IGBTs (insulated gate bipolar transistors) led to new microcomputer-controlled power supplies that automatically adjust the operating frequency to the resonance frequency of the circuit formed by the capacitance of the electrode configuration and the inductance of the secondary winding of the HV transformer. Special power supplies were developed to generate repetitive pulse trains resulting in improved statistical distribution of the microdischarges across the surface, a prerequisite for more uniform treatment.[32,212] Further improvements can be expected from new solid-state devices using IGCTs (integrated gate commutated thyristors) that can switch up to 5 MVA at 10 kV. This way the use of bulky high-voltage transformers can be eliminated altogether.

The result of this atmospheric-pressure plasma treatment is similar to that obtained in low-pressure oxygen discharges, a substantial increase of surface energy. For plastic foils changes from about 20–30 mJ/m^2, typical values for untreated polymers, to 50–70 mJ/m^2 have been reported. This is a very desirable effect because the higher the surface energy, the more wettable the material. Plasma treatment thus enhances adhesion, printability and dye uptake. Recent investigations also include the upgrading of wool and textiles and the plasma treatment of insulated wires and cables. In this special application pretreatment of the surface without damage to the insulation is required before permanent marking becomes possible.

During surface activation radicals formed in the plasma disrupt chemical bonds in the surface layer causing the formation of new species with different properties. This results in a modification of the near-surface region without changing the desirable bulk properties of the material.[213,214] In air plasmas the active species were identified as oxygen atoms resulting in the buildup of oxygenated carbon centers in the surface layer. XPS spectra of plasma treated LDPE (low density polyethylene) revealed an oxygen/carbon ratio up 30% after plasma treatment.[215]

If different gas environments are chosen also the incorporation of other atoms like N, F, Si, etc. is possible. Traditionally this has been achieved in the closed chamber of a low-pressure glow discharge.[216–219] Progress in

purging and sealing techniques (Fig. 11) made it possible to use such environments and special gas mixtures also on installations with fast moving webs operating at atmospheric pressure.[32,212]

Special interest has also been devoted to reactive gas mixtures that lead to the deposition of extremely thin coatings with improved wettability or other desired properties. Polymer, and SiO_x coatings[219–223] or even hard diamond-like carbon films[224,225] have been obtained in dielectric-barrier discharges.

Also the removal of photoresist layers in lithographic processes was investigated.[226] The possibility to modify, etch or coat surfaces at low temperature and close to atmospheric pressure is an important advantage for large-scale industrial applications. The main advantage is that no expensive evacuation systems are required. It is to be expected that coating techniques using vapor or gas phase deposition in DBDs and also the annealing and oxidation of sol-gel films subjected to such discharges will be further developed.

A more recent development, still at the laboratory stage, is the modification of surfaces and thin film deposition in spatially homogeneous, diffuse atmospheric-pressure discharges.[33–35,227–230] The spatial homogeneity of dielectric-barrier discharges can be influenced by using two dielectric barriers and specially shaped metal electrodes,[231] by carefully selecting the gap width and operating frequency, and by using large fractions of helium or neon.[232,233] Also certain additives like traces of acetone or methane in argon have an influence.[234]

Investigations employing modern surface analysis testify improved properties, similar to the best obained in low-pressure glow discharges, if spatially homogeneous rather than filamentary dielectric-barrier discharges

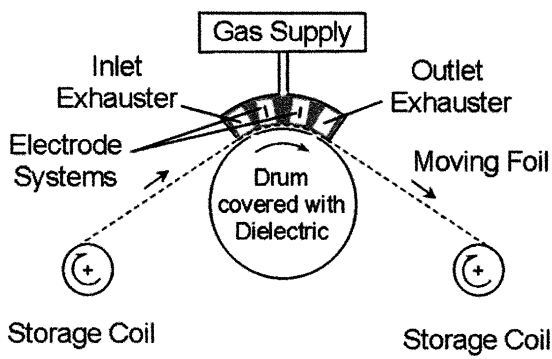

Fig. 11. Online surface treatment with reactive gases (after Refs. 32, 212).

are used.[215,235,236] Relative recent investigations on low-current-density, diffuse dielectric-barrier discharges also suggest novel applications of mild plasmas for sterilization and disinfection purposes[237–239] and for selectively influencing biological cells.[240] If reliable control of these diffuse discharges can be obtained in an industrial environment, further applications of dielectric-barrier discharges for surface modification are to be expected.

6. SD CO_2 LASERS

Based on their experience with dielectric-barrier discharges in ozone generators Yagi and co-workers[241–244] developed their SD CO_2 laser (SD stands for silent discharge). This high-power infrared laser ($\lambda = 10.6\,\mu$m), used for precision welding and cutting of thick metal plates, soon became a commercial success. Contrary to other commercial high-power CO_2 lasers that operate at 13.65 MHz or 27.3 MHz, the SD laser uses rather low frequencies between 50 kHz and 200 kHz. The advantage of the low frequency is that the dielectric layers on the electrodes (glass or alumina) effectively limit the discharge current and stabilize the discharge. Another advantage is the availability of inexpensive, highly efficient solid-state power supplies.

Operating at reduced pressure (5–20 kPa) in a mixture of $N_2/He/CO_2/CO$ (60/28/8/4) the discharge looks fairly homogeneous. Since there is not enough time to remove residual ions between half waves, the plasma essentially acts as a resistive load with modulated conductivity (ion dragging mode). The laser performance was optimized by choosing a wide discharge gap of 4–5 cm spacing and by using this unusually high nitrogen content.[245] A strong transverse gas flow at a velocity of 50–80 m/s provides discharge stabilization and cooling. Output powers reach 5–20 kW. The efficiency in the TM_{00} mode is about 10%. Within a few years this SD CO_2 laser has gained a substantial market share in Japan. More recently, also sealed operation of CO_2 lasers pumped by dielectric-barrier discharges at 600 kHz has been proposed.[246]

7. ULTRAVIOLET EXCIMER LAMPS AND MERCURY-FREE FLUORESCENT LAMPS

In dielectric-barrier discharges the plasma conditions in the microdischarges, resembling those of high-pressure glows, are ideally suited to induce excimer formation. Appropriate gas mixtures can be sealed in silica glass vessels to make fairly simply excimer lamps, efficient and powerful sources of ultraviolet (UV) or vacuum ultraviolet (VUV) radiation (Fig. 12).

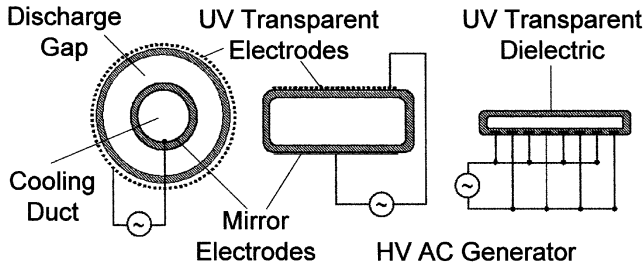

Fig. 12. Sealed cylindrical and planar excimer lamp configurations (Ref. 277).

Long lifetimes can be obtained since the electrodes are not in contact with the plasma. Metal deposition on the walls and electrode erosion, processes that normally limit the lifetime of lamps, are avoided. To extract as much radiation from the plasma volume as possible the front electrode is perforated, or a wire mesh is used. Both solutions provide up to 90% transmission. The rear electrode can be used as a mirror. The configuration in the right part of Fig. 12 uses co-planar electrodes of alternating polarity. This way surface discharges are initiated that have similar properties to those of the microdischarges bridging the discharge gap.

A large number of excimers have been obtained in dielectric-barrier discharges.[247] Table I gives a selection of wavelengths obtained, covering the range from 126–354 nm. The most important excimer lamps are those based on rare gas dimers and the rare gas halides known from excimer lasers.

7.1. Excimer Lamps Based on Rare Gas Dimers

The first excimer lamps mentioned in the literature were small VUV sources used for spectroscopic purposes.[248–250] The relatively broad second excimer continua of the rare gases were used as background radiation for absorption measurements in the VUV range between 70 and 180 nm. During the last decade powerful efficient VUV excimer lamps were developed that have found novel important industrial applications. Dielectric-barrier discharges in high density rare gases operated at about 0.1 MPa can efficiently

Table I. Selection of Excimers Obtained in Dielectric-barrier Discharges and their Respective Peak Wavelengths in nm (Commercially Available Lamps in Thick Print)

$\mathbf{Ar_2^*}$	$\mathbf{Kr_2^*}$	F_2^*	$\mathbf{Xe_2^*}$	ArCl*	ArF*	**KrCl***	KrF*	XeI*	Cl_2^*	XeBr*	Br_2^*	**XeCl***	I_2^*	XeF*
126	**146**	157	**172**	175	193	**222**	248	253	259	282	289	**308**	342	354

convert electron kinetic energy in electronic excitation energy. Due to high collision rates this excitation is rapidly funneled to a few low lying atomic and dimer levels. The dimer Xe_2^* is formed in a three-body reaction involving excited and ground state Xe atoms. Computations indicate that under favorable conditions 40–80% of the discharge power can be converted to VUV radiation concentrated in the second excimer continua of Ar, Kr or Xe.[251–257] The observed emission results from the lowest two dimer states $Xe_2^*(^1\Sigma_u^+, ^3\Sigma_u^+)$ which decay predominantly by radiation concentrated in a narrow wavelength region of 10–15 nm half width around the peak wavelengths given in Table I. Best results are obtained with short-pulse excitation. Since the shorter wavelengths of Ar_2^* and Kr_2^* require special window materials (MgF_2, LiF, CaF_2) to extract the VUV radiation the xenon excimer lamp became the most important one. Its radiation, peaking at 172 nm, is transmitted by the walls of high purity silica (Suprasil) vessels. The highest VUV efficiency of commercial xenon excimer lamps is quoted to reach 40%. To overcome the problems with window materials at short wavelengths also open or windowless excimer systems have been proposed.[258,259] In these systems the (dielectric-coated) electrodes and the sample to be irradiated are placed in a chamber with an excimer forming gas mixture like, e.g., Ar. The sample is subjected to VUV radiation from the discharge region without intermediate windows. Recent experiments with a 0.3-m wide electrode system purged with atmospheric-pressure Ar demonstrated VUV induced surface modification on a technical scale through photo polymerization of thin acrylate films on moving polymer foils.[260]

7.2. Excimer Lamps Based on Rare Gas Halide Excimers

The halogen dimers and rare gas halide excimers listed in Table I show much narrower emission features, typically a single emission peak of 2–4 nm half width. The most important lamp of this category is the XeCl* excimer lamps delivering practically monochromatic radiation at 308 nm. The predominant reaction path leading to the formation of the exciplex XeCl* under such conditions is the recombination of Xe^+ and Cl^- ions. Sealed lamps of several kW electrical power and narrow-band UV output of about 1 kW are on the market. For UV curing applications on printing machines tubular XeCl* lamps up to 2 m length are available. Since F atoms attack silica surfaces, KrF*, ArF*, and F_2^* lamps have only been used in through-flow systems in the laboratory.[261–263] For sealed lamps the development of internal protective coatings (MgF_2, LiF) would be required. Powerful and efficient XeBr* and XeI* lamps, on the other hand, have successfully been tested in the laboratory[264,265] and will soon be introduced

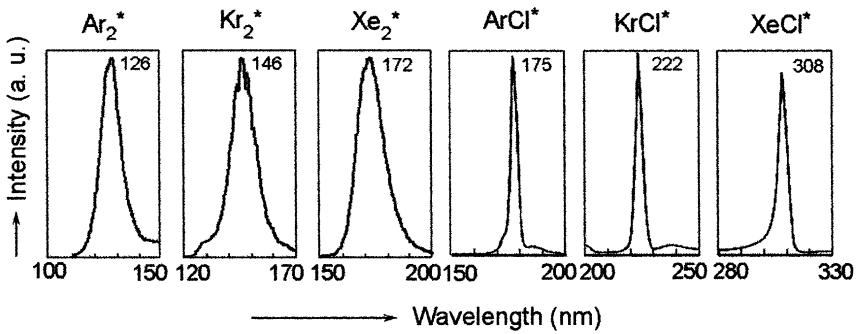

Fig. 13. Emission spectra of various excimer lamps (Ref. 25).

to the market. Using pulsed discharges also high-power excimer flash lamps were investigated.[266–272] Since excimer formation works up to fairly high power densities in the plasma (10^7 Wcm^{-3}), UV peak powers of several MW and average UV powers in the kW range have been obtained.

In general in can be stated that the use of dielectric-barrier discharges to generate VUV or UV excimer radiation has proved to be a very useful concept.[25–30,32,247,251,273–277] Excimer lamps produce high-intensity narrow-band radiation at various UV and VUV wavelengths. Their efficiencies reach 10–40%. The use of excimers has several advantages. High photon fluxes can be extracted from the plasma without self-absorption. Many properly optimized excimer forming gas mixtures exhibit only one dominant narrow emission band. Commercial sealed lamps use external electrodes and can be operated near room temperature if adequate cooling is used. Typical filling pressures are in the range 10^4 to 10^5 Pa, typical discharge gap widths in the range of 0.1 to 5 mm. The operating frequency can be between line frequency and microwave frequencies, but is normally chosen to lie between 20 kHz and 500 kHz. For this frequency range compact and efficient switch-mode power supplies are available. Since at about atmospheric pressure excimer formation and decay are extremely fast processes and no preheating of the gas mixture is required excimer lamps can be pulsed and gated at a fast rate.

7.3. Applications of Excimer UV Lamps

Based on high-intensity UV radiation from excimer lamps a number of industrial applications have emerged. A relative straightforward application is the replacement of hot medium-pressure mercury lamps in UV curing processes on printing machines.[278] For this application, especially used for

high-speed printing on heat sensitive substrates, XeCl* lamps or combinations of XeCl* and KrCl* are used. Novel applications were established for the VUV radiation of the Xe_2^* excimer lamp. The energy of its 172-nm photons corresponds to 7.2 eV, which is high enough to break most molecular bonds. Examples are the generation of $O(^3P)$ and $O(^1D)$ atoms in oxygen or air, of $O(^1D)$ from N_2O and OH radicals in water and in humid gas streams. Large numbers of xenon excimer lamps are now routinely used for "UV cleaning" of substrates in display and semiconductor manufacturing. The cleaning action, used as a means to remove hydrocarbon residues after chemical rinses, is attributed to the action of oxygen atoms. The atoms participate in chemical reactions of VUV photons with the residues to form volatile products like CO, CO_2, and H_2O. Novel applications of excimer UV lamps have also been propagated for pollution control[279] and water treatment.[280] Advanced oxidation processes resulting in oxidative degradation following VUV photolysis of air or water as well as direct UV/VUV photocleavage of pollutants are possible destruction mechanisms. Many of the common pollutants (CCl_4, CH_3Cl, ClHC=CHCl, $ClHC=CCl_2$, $Cl_2C=CCl_2$) strongly absorb at wavelengths around 200 nm. Their absorption coefficients can be well in excess of 10^{-17} cm^2/molecule, more than six orders of magnitude larger than those of oxygen or water in this wavelength region. Consequently, selective destruction of micropollutants at very low concentrations can be achieved.[279]

By UV-induced decomposition of properly selected precursor substances photo-deposition of large-area or patterned thin metal films,[27,32,273,281] insulating layers with extremely high[282,283] or low[284,285] dielectric constants, or also semiconductor films has been demonstrated.[27,277,286] This has been achieved with gas phase precursors, liquid films or sol gel films. Also the photo-etching and structuring of polymer surfaces[273,287–290] and the photo-assisted low-temperature oxidation of Si, SiGe, and Ge at 250–400°C has been reported.[277,291,292] Very recently also rapid photo-oxidation of Si at room temperature was achieved with Ar_2^* excimer radiation peaking at 126 nm.[293] It is quite evident that the availability of reliable and affordable sources of VUV radiation provides a new stimulus to photochemistry in general and especially to materials processing in semiconductor manufacturing. Photons and free radicals generated by UV radiation can be used for surface treatment in a similar way as free radicals generated in a plasma. For example, irradiation of hydrophobic PTFE (polytetrafluoroethylene, Teflon) with xenon or krypton excimer lamps under ammonia atmosphere results in hydrophilic surfaces. The changes are attributed to the incorporation of nitrogen and hydrogen atoms into the surface.[294] In general it can be stated that photon induced chemical reactions are much more selective than plasma attack and that patterning

is much simpler with optical radiation. Low cost, high-power excimer lamp systems can thus provide an interesting alternative plasma treatment and to expensive excimer lasers.[295] This is especially the case when large substrates have to be modified.

7.4. Mercury-free Fluorescent Lamps and Flat Panels

UV photons can also be utilized to excite phosphors that convert UV radiation to visible light. This principle is used on a large scale in fluorescent lamps and energy saving lamps. In these light sources the mercury line radiation ($\lambda = 254$ nm) of a low-pressure glow discharge is used to generate white light from a mixture of phosphors coated on the interior surface of the lamp. The advent of excimer lamps provided the possibility to discard the metal electrodes in the discharge space and to produce mercury-free fluorescent lamps in a variety of shapes, including cylindrical lamps and planar light panels. The highly efficient Xe_2^* radiation at 172 nm is used to replace the Hg line radiation. A very successful product development resulted in small cylindrical lamps (Fig. 14) used in a new generation of scanners and copying machines. These information processing lamps operate with external electrodes in a mixture of Ne and Xe at a frequency of about 20 kHz. Ne is used as a buffer gas to reduce the ignition voltage and, of course, to reduce costs. About 10% Xe is enough to obtain the well-known second excimer continuum of Xe. Since only visible or near UV radiation is emitted from the lamp it can be made of glass. The main advantage of these new fluorescent lamps is that they can be switched on fast and

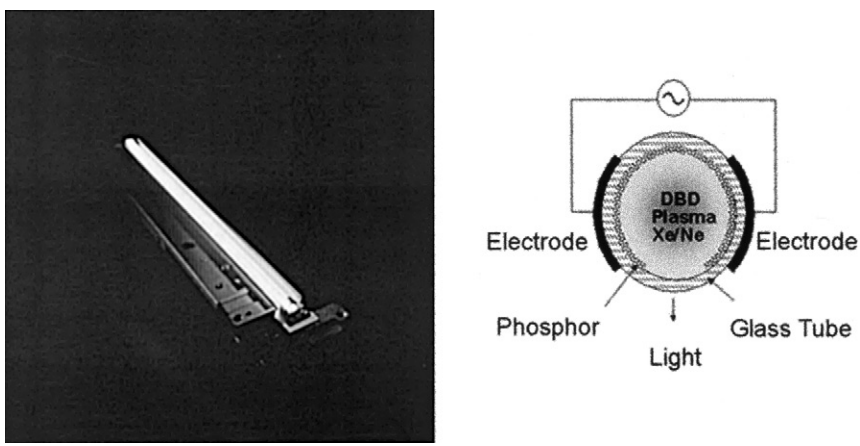

Fig. 14. Fluorescent lamp based on Xe excimers (USH10).

that no warming up or idling is required. In scanners and copiers the lamp is only active during the scan, which results in very long periods between lamp replacement.

In addition flat planar white-light panels have been proposed[296,297] and developed.[298] They have found applications as background illumination in LCDs (liquid crystal displays) and in industrial, medical, and transportation displays. Extremely thin, flat commercial light panels, having a thickness of only 10 mm, are now available in the size range 15–30 in. diagonal. They are much brighter (up to 10,000 cd/m^2) as conventional backlighting systems using multiple mercury lamps and reach lifetimes up to 100,000 hr. Coplanar electrode systems are used similar to that shown in the right part of Fig. 12 in combination with an internal phosphor coating. A typical sealed flat panel is made of two parallel glass substrates, a surrounding glass frame and multiple spacers that support the structure during evacuation and filling.

Electrodes, dielectric barriers, reflecting and phosphor layers are deposited by thick film printing, relatively inexpensive production techniques. The printed electrode lines are specially designed to facilitate ignition and to fix the microdischarges at certain locations. The electrode layer is covered by a thin dielectric barrier. To enhance efficiency, these flat panels use repetitive short-pulse excitation and to enhance discharge stability the filling pressure is lowered to about 10 kPa. Contrary to mercury lamps these excimer-based fluorescent lamps produce no hazardous waste. In addition, they avoid an important ageing problem, the incorporation of mercury into the phosphor layer.

8. PLASMA DISPLAY PANELS (PDPs)

AC plasma displays utilizing Xe VUV radiation to excite phosphors are the most recent addition to dielectric-barrier discharge applications.[299,300] Within a few years they reached market values by far surpassing those of all other DBD applications. The original idea to use dielectric-barrier discharges for large-area displays originated at the University of Illinois at Urbana-Champlaign in 1964.[301] Bitzer and Slottow, two professors at that institution, were engaged in computer-based education and were looking for a graphic display of their computer outputs. They took a matrix of individually addressable tiny dielectric-barrier discharge cells filled with a Penning mixture of Ne and traces of Ar.[302] This first monochromatic plasma display already achieved a resolution of 512×512 pixels and prudently utilized the inherent memory effect due to surface charges on the walls. The physics of this effect had previously been investigated and discussed by Loeb and El Baccal[303] following earlier the work of Harries and von Engel.[304] Efforts

to find gases emitting additional colors to the orange Ne lines were not very successful. Multicolor operation based on photo excited phosphors was demonstrated as early as 1973 with a 1024×1024 panel.[305] Further progress towards a color plasma display was only made when Xe VUV radiation was utilized to excite phosphor layers deposited inside the tiny gas discharge cells used for individual pixels. To obtain sufficient visible radiation from such a small volume it is essential to raise the pressure to values where efficient excimer formation occurs, typically about 50–70 kPa. Higher pressure favors excimer formation. Above 10 kPa the three-body reaction of excited Xe* atoms with two ground state atoms to form Xe_2^* becomes faster than radiative decay of Xe*. The formation of the Xe_2^* excimer occurs even when up to 95% of He or Ne are used as buffer gases. In addition to lower costs this has the advantage of lowering the ignition voltage to values suitable for integrated transistor drivers. In the tiny gas cells of about 0.1 mm width and height the plasma emission consists of the 147 mm Xe resonance line, of the first excimer continuum around 150 nm and, predominantly, of the second excimer continuum around 172 nm. While the resonance line is subject to radiation absorption, the excimer radiation can escape from the plasma with practically no absorption. Adjacent cells are separated by barrier ribs to reduce cross talk (see Fig. 15c).

In every cell the VUV radiation excites red, green, or blue internal phosphor coatings. Each cell acts as a miniature fluorescent lamp. The discharge cells are grouped as RGB (red, green, blue) color triplets or quadruplets (RGBG). A large display has up to 1280 by 1024 such image points. Two sets of perpendicularly arranged thin electrode strips allow addressing of individual cells. The electrodes are deposited on two parallel glass plates on opposite sides of the gas space or in a co-planar configuration on one glass plate. In this case a trigger electrode is used on the opposite side. In ac plasma displays all electrodes are covered by dielectric layers and sputter resistant MgO coatings. This material has also an extremely high coefficient for secondary electron emission caused by impinging Ne^+ or He^+ ions, which helps in lowering the breakdown voltage. The discharge is sustained by a square-wave voltage of 50–100 kHz frequency. At every polarity change a short current pulse of about 20 ns duration is initiated in the cell resulting in a short VUV pulse. The average intensity of each cell can be adjusted by duty cycle modulation.

With this technology bright displays with close to 17 million color shades and contrast ratios up to 3000:1 can now be realized. The peak luminance has reached 750 cd m^{-2}. It is interesting to note that it took more than 20 years between the invention of the plasma display and the technological breakthrough that allowed mass production of large flat wall-hung color TV sets. With about 200,000 sets sold in the year 2000 and up to 7

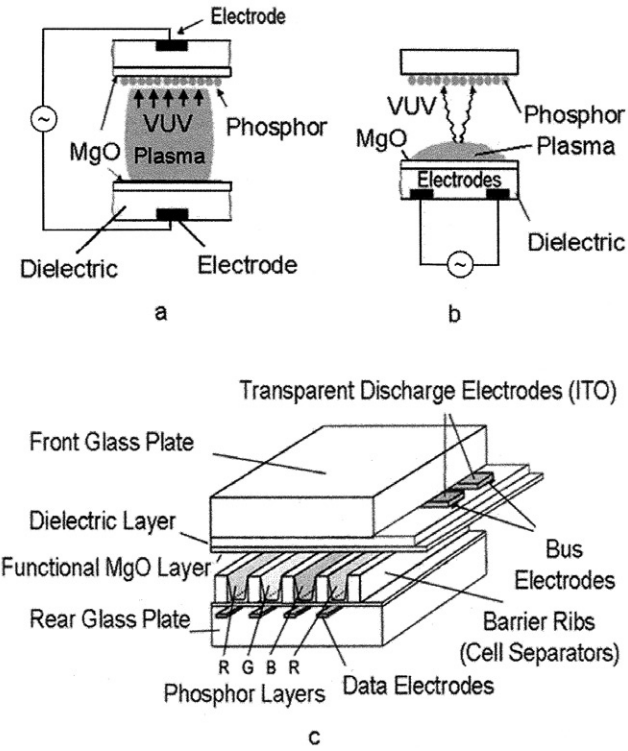

Fig. 15. Pixel cells with opposite (a) and co-planar (b) electrodes and complete plasma display configuration (c). (RGBR: red, green, blue, red).

million sets anticipated for 2005, PDPs are expected to surpass an annual market value of US$ 10 billion. Production facilities for flat plasma displays have been built in Japan, South Korea, and Taiwan, more recently also in China and India. Intrinsic advantages of PDPs include distortion-free crystal clear pictures, large screen sizes, and wide viewing angles. They can display digital high definition television (HDTV) pictures and can be directly linked to video, audio, and DVD equipment.

The manufacturing of plasma displays profits from relatively inexpensive materials, moderate clean room requirements, and comparatively simple, high throughput thick film processes. Recent technological advances increased the resolution, luminance, and lifetime by alternatively displaying even and odd lines. The cost of the drive circuitry could be substantially reduced by limiting the drive voltage to about 80 V without reducing the discharge voltage. Screen sizes between 0.6 m and 1.6 m diagonal are available. The thickness of the complete panel is between 4 and 12 cm, the thickness of the sealed glass discharge cell only 0.6 cm. It is expected that this

technology will eventually replace bulky cathode ray tubes in many television and large-area monitor applications.

Presently, the efficiency of converting electrical power to visible radiation is rather low, in the range of 1%. Detailed measurements and modeling efforts have led to a satisfactory understanding of the physical processes in a pixel cell. As an example, the energy losses in a mixture of 10% Xe in 66 kPa Ne were determined by Revel *et al.*[306] using numerical modeling. Only 15% of the power is spent on the excitation of Xe atoms, the rest on ion acceleration, Ne excitation and Xe and Ne ionization. This results in a 10% UV efficiency of which 40% can be collected on the phosphor. From this fraction about 30% is converted to visible light resulting in total luminous efficiency of only 1 lm/W. Clearly such models will be used to further improve PDP performance by identifying more favorable electrode configurations, cell geometries, gas composition and excitation mechanisms. The other hope is to develop more efficient phosphors for the conversion of VUV radiation. From an energy standpoint it should be possible to convert one VUV photon to two visible photons. Recent investigations indeed succeeded in converting VUV photons into red radiation with a quantum efficiency approaching two.[307] If similar progress can be reached for green and blue phosphors this could practically double the efficiency of present PDPs.

9. CONCLUSION AND OUTLOOK

Industrial applications of dielectric-barrier discharges have come a long way and, more recently, have substantially increased their market penetration. No doubt, this trend will continue. Several reasons can be given for this renaissance of an in principle rather old gas discharge. Obviously, our understanding of the fundamental processes determining discharge initiation and the ensuing plasma chemical reactions has profited from modern modeling and diagnostic tools. An important aspect is the availability of reliable cross sections on electron collisions in various gases and of recommended values for rate coefficients of various transient species. The development and cost reduction of modern power electronics and the engineering skills of matching power supplies to DBD properties were of equal importance. Miniaturization of electrode structures and discharge cells and finding affordable large-throughput manufacturing technologies resulted in an explosive growth of novel applications in display devices.

Clearly these recent achievements will open roads to additional new applications. Microstructured DBDs can be used for large-area plasma electrodes or as a laboratory on the microchip for diagnosic purposes.[308] Further progress is expected from using ultra short pulses,[52,56,309] dielectrics with special properties and from a better understanding of the surface

discharges which represent an integral aspect of all dielectric-barrier discharges.[310]

ACKNOWLEDGMENT

Thanks are due to the University of Minnesota at Minneapolis. Work on this review article began while the author stayed at the Department of Mechanical Engineering during spring 2001.

REFERENCES

1. W. Siemens, *Poggendorff's Ann. Phys. Chem.* **102**, 66 (1857).
2. T. Andrews and P. G. Tait, *Phil. Trans. Roy. Soc.* (*London*) **150**, 113 (1860).
3. P. Hautefeuille and J. Chappuis, *Compt. Rend. Acad. Scé.* (*Paris*) **92**, 80 (1881).
4. E. Warburg and G. Leithäuser, *Ann. Physik* (4) **28**, 313 (1909).
5. E. Warburg, *Ann. Physik* (4) **13**, 464 (1904).
6. E. Warburg, *Z. Tech. Phys.* **6**, 625 (1925).
7. H. Becker, *Wiss. Veröff. Siemens-Konzern* **1**, 76 (1920).
8. H. Becker, *Wiss. Veröff. Siemens-Konzern* **3**, 243 (1923).
9. M.-P. Otto, *Bull. Soc. Franç. Electr.* **9**, 129 (1929).
10. K. Buss, *Arch. Elektrotech.* **26**, 261 (1932).
11. A. Klemenc, H. Hinterberger, and H. Höfer, *Z. Elektrochem.* **43**, 708 (1937).
12. M. Suzuki, *Proc. Jpn. Acad.* **26**, 20 (1950).
13. M. Suzuki and Y. Naito, *Proc. Jpn. Acad.* **28**, 469 (1952).
14. K. Honda and Y. Naito, *J. Phys. Soc. Jpn.* **10**, 1007 (1955).
15. H. Gobrecht, O. Meinhardt, and F. Hein, *Ber. Bunsenges. f. phys. Chem.* **68**, 55 (1964).
16. M. A. Bagirov, M. A. Kurbanov, A. V. Shkilev, and N. E. Nuraliev, *Sov. Phys.-Tech. Phys.* **16**, 1011 (1971).
17. T. C. Manley, *Trans. Electrochem. Soc.* **84**, 83 (1943).
18. E. Briner and B. Susz, *Helv. Chim. Acta.* **13**, 678 (1930).
19. Yu. V. Filippov, V. A. Boblikova, and V. I. Panteleev, *Electrosynthesis of Ozone*, Moscow State University (1987) (in Russian).
20. J. C. Devins, *J. Electrochem. Soc.* **103**, 460 (1956).
21. R. W. Lunt, *Adv. Chem. Ser.* **21**, 286 (1959).
22. S. Fuji and N. Takemura, *Adv. Chem. Series* **21**, 334 (1959).
23. V. G. Samoilovich, V. Gibalov, and K. V. Kozlov, *Physical Chemistry of the Barrier Discharge* (J. P. F. Conrads and F. Leipold, eds.), DVS-Verlag, Düsseldorf (1997) (Original Russian version: Moscow State University, 1989).
24. U. Kogelschatz, in *Proc. 16th Int. Conf. on Phenomena in Ionized Gases (XVI ICPIG)*, Düsseldorf (1983), Invited Papers, pp. 240–250.
25. B. Eliasson and U. Kogelschatz, *IEEE Trans. Plasma Sci.* **19**, 309 (1991).
26. B. Eliasson and U. Kogelschatz, *IEEE Trans. Plasma Sci.* **19**, 1063 (1991).
27. U. Kogelschatz, in *Proc. 10th Int. Conf. on Gas Discharges and their Applications (GD-92)*, Swansea, UK (1992), Vol. II, pp. 972–982.
28. B. Eliasson, W. Egli, and U. Kogelschatz, *Pure Appl. Chem.* **66**, 1275 (1994).
29. U. Kogelschatz, B. Eliasson, and W. Egli, *J. Phys. IV* (*France*) **7**, C4–47 (1997).
30. U. Kogelschatz, B. Eliasson, and W. Egli, *Pure Appl. Chem.* **71**, 1819 (1999).

31. U. Kogelschatz, Ozone generation and dust collection, in *Electrical Discharges for Environmental Purposes: Fundamentals and Applications* (E. M. van Veldhuizen, ed.), Nova Science Publishers, Commack, New York (2000), Chapter 12, pp. 315–344.
32. U. Kogelschatz and J. Salge, High pressure plasmas. Dielectric-barrier and corona discharges: Properties and technical applications, in *Low Temperature Plasma Physics: Fundamental Aspects and Applications* (R. Hippler, S. Pfau, M. Schmidt, and K. H. Schoenbach, eds.), Wiley–VCH, Weinheim (2001), Chapter 13, pp. 331–357.
33. K. G. Donohoe and T. Wydeven, *J. Appl. Polymer Sci.* **23**, 2591 (1979).
34. S. Kanazawa, M. Kogoma, T. Moriwaki, and S. Okazaki, *J. Phys. D: Appl. Phys.* **21**, 838 (1988).
35. F. Massines, A. Rabehi, P. Decomps, R. B. Gadri, P. Ségur, and C. Mayoux, *J. Appl. Phys.* **83**, 2950 (1998).
36. D. G. Boyers and W. A. Tiller, *Appl. Phys. Lett.* **41**, 28 (1982).
37. E. Ammelt, D. Schweng, and H.-G. Purwins, *Phys. Lett. A* **179**, 348 (1993).
38. W. Breazeal, K. M. Flynn, and E. G. Gwinn, *Phys. Rev. E* **52**, 1503 (1995).
39. U. Kogelschatz, Filamentary, patterned and diffuse barrier discharges, *IEEE Trans. Plasma Sci.* **30** (2002), accepted for publication.
40. K. Yoshida and H. Tagashira, *Memoirs Kitami Inst. Technol.* **18**, 11 (1986).
41. B. Eliasson, M. Hirth, and U. Kogelschatz, *J. Phys. D: Appl. Phys.* **20**, 1421 (1987).
42. D. Braun, U. Küchler, and G. Pietsch, *J. Phys. D: Appl. Phys.* **24**, 564 (1991).
43. D. Braun, V. Gibalov, and G. Pietsch, *Plasma Sources Sci. Technol.* **1**, 166 (1992).
44. V. I. Gibalov and G. Pietsch, *Russ. J. Phys. Chem.* **68**, 839 (1994).
45. W. Egli, J. M. Favre, and B. Eliasson, *Crosscuts* **7**(3), 14 (1998).
46. G. Steinle, D. Neundorf, W. Hiller, and M. Pietralla, *J. Phys. D: Appl. Phys.* **32**, 1350 (1999).
47. J. Dřímal, V. I. Gibalov, and V. G. Samoilovich, *Czech. J. Phys.* **B37**, 1248 (1987).
48. J. Dřímal, K. V. Kozlov, V. I. Gibalov, and V. G. Samoilovich, *Czech. J. Phys. B* **38**, 159 (1988).
49. V. I. Gibalov, J. Dřímal, M. Wronski, and V. G. Samoilovich, *Contrib. Plasma Phys.* **31**, 89 (1991).
50. E. Gerova and S. Müller, in *Proc. 23rd Int. Conf. on Phenomena in Ionized Gases (XXIII ICPIG)*, Toulouse, France (1997), Vol. 4, pp. 120–121.
51. R. Wendt and H. Lange, *J. Phys. D: Appl. Phys.* **31**, 3368 (1998).
52. C. Hilbert, I. Gaurand, O. Motret, and J. M. Pouvesle, *J. Appl. Phys.* **85**, 7070 (1999).
53. C. Lukas, M. Spaan, V. Schulz-von der Gathen, M. Thomson, R. Wegst, H. F. Döbele, and M. Neiger, *Plasma Sources Sci. Technol.* **10**, 445 (2001).
54. K. V. Kozlov, H.-E. Wagner, R. Brandenburg, and P. Michel, *J. Phys. D: Appl. Phys.* **34**, 3164 (2001).
55. K. Kunze, M. Miclea, G. Musa, J. Franzke, C. Vadla, and K. Niemax, *Spectrochimica Acta* **B57**, 137 (2002).
56. O. Motret, C. Hibert, S. Pellerin, and J. M. Pouvesle, *J. Phys. D: Appl. Phys.* **33**, 1483 (2000).
57. M. Spaan, J. Leistikow, V. Schulz-von der Gathen, and H. F. Döbele, *Plasma Sources Sci. Technol.* **9**, 146 (2000).
58. N. K. Bibinov, A. A. Fateev, and K. Wiesemann, *Plasma Sources Sci. Technol.* **10**, 579 (2001).
59. A. V. Phelps and S. A. Lawton, *J. Chem. Phys.* **69**, 1055 (1978).
60. N. P. Penkin, V. V. Smirnov, and O. D. Tsygir, *Sov. Phys.: Techn. Phys.* **27**, 945 (1982).
61. B. Eliasson, U. Kogelschatz, and P. Baessler, *J. Phys. B: At. Mol. Phys.* **17**, L797 (1984).
62. B. Eliasson and U. Kogelschatz, *J. Phys. B: At. Mol. Phys.* **19**, 1241 (1986).

63. S. Kajita, S. Ushirosa, and Y. Kodo, *J. Appl. Phys.* **67**, 4015 (1990).
64. P. C. Cosby, *J. Chem. Phys.* **98**, 9560 (1993).
65. A. V. Phelps and L. C. Pitchford, *Phys. Rev. A* **31**, 2932 (1985).
66. P. C. Cosby, *J. Chem. Phys.* **98**, 9544 (1993).
67. W. L. Nighan, *Phys. Rev. A* **2**, 1989 (1970).
68. A. N. Lobanov and A. N. Suchkov, *Sov. J. Quant. Electron.* **4**, 843 (1975).
69. H. N. Kücükarpaci and J. Lucas, *J. Phys. D: Appl. Phys.* **12**, 2123 (1979).
70. M. Braglia, R. Winkler, and J. Wilhelm, *Contrib. Plasma Phys.* **31**, 463 (1991).
71. B. Eliasson, F.-G. Simon, and W. Egli, Hydrogenation of CO_2 in a silent discharge, in *Non-Thermal Plasma Techniques for Pollution Control*, NATO ASI Series, Vol. G 34, Part B (B. M. Penetrante and S. E. Schultheis, eds.), Springer, Berlin (1993), pp. 321–337.
72. A. C. Gentile, *Kinetic Processes and Plasma Remediation of Toxic Gases*, PhD Thesis, University of Illinois at Urbana-Champaign (1995), ftp://uigelz.ece.uiuc.edu/pub/theses/gentile-thesis.pdf
73. R. Dorai and M. J. Kushner, *J. Appl. Phys.* **88**, 3739 (2000).
74. X. Xu, *Dynamics of high- and low-pressure plasma remediation*, PhD Thesis, University of Illinois at Urbana-Champaign (2000), ftp://uigelz.ece.uiuc.edu/pub/theses/xxu_thesis.pdf
75. I. Stefanović, N. K. Bibinov, A. A. Deryugin, I. P. Vinogradov, A. P. Napartovich, and K. Wiesemann, *Plasma Sources Sci. Technol.* **10**, 406 (2001).
76. X. P. Xu and M. J. Kushner, *J. Appl. Phys.* **84**, 4153 (1998).
77. R. C. Campbell, R. Veerasingam, and R. T. McGrath, *IEEE Trans. Plasma Sci.* **23**, 698 (1995).
78. J.-P. Boeuf and L. C. Pitchford, *IEEE Trans. Plasma Sci.* **24**, 95 (1996).
79. J.-P. Boeuf and H. Doyeaux, *Europhys. News* **27**, 46 (1996).
80. Y. Ikeda, J. P. Verboncoeur, P. J. Christenson, and C. K. Birdsall, *J. Appl. Phys.* **86**, 2431 (1999).
81. H. S. Jeong, B.-J. Shin, and K.-W. Whang, *IEEE Trans. Plasma Sci.* **27**, 171 (1999).
82. T. Tamida, S. J. Sanders, and M. Tanaka, *Jpn. J. Appl. Phys.* **39**, 583 (2000).
83. B. Eliasson and W. Egli, *Helv. Phys. Acta* **60**, 241 (1987).
84. J. J. Coogan and A. D. Sappey, *IEEE Trans. Plasma Sci.* **24**, 91 (1996).
85. U. Kogelschatz, Advanced ozone generation, in *Process Technologies for Water Treatment* (S. Stucki, ed.), Plenum Press, New York, NY (1988), pp. 87–120.
86. Z. Falkenstein and J. J. Coogan, *J. Phys. D: Appl. Phys.* **30**, 817 (1997).
87. T. Tamida, A. Iwata, J. Nishimae, and M. Tanaka, in *Proc. 12th Int. Conf. on Gas Discharges and Their Appl. (GD 97)*, Greifswald (1997), Vol. II, pp. 641–644.
88. C. F. Schönbein, *Poggendorff's Ann. Phys. Chem.* **50**, 616 (1840).
89. U. Kogelschatz, B. Eliasson, and M. Hirth, *Ozone Sci. Eng.* **10**, 367 (1988).
90. R. Peyrous, P. Pignolet, and B. Held, *J. Phys. D: Appl. Phys.* **22**, 1658 (1989).
91. G. Pietsch and V. I. Gibalov, *Pure Appl. Chem.* **70**, 1169 (1998).
92. J. Kitayama and M. Kuzumoto, *J. Phys. D: Appl. Phys.* **30**, 2453 (1997).
93. S. Yagi and M. Tanaka, *J. Phys. D: Appl. Phys.* **12**, 1509 (1979).
94. V. G. Samoilovich and V. I. Gibalov, *Russ. J. Phys. Chem.* **60**, 1107 (1986).
95. D. Braun, U. Küchler, and G. Pietsch, *Pure Appl. Chem.* **60**, 741 (1988).
96. I. A. Kossyi, A. Yu. Kostinsky, A. A. Matveyev, and V. P. Silakov, *Plasma Sources Sci. Technol.* **1**, 207 (1992).
97. J. Kitayama and M. Kuzumoto, *J. Phys. D: Appl. Phys.* **32**, 3032 (1999).
98. J. T. Herron, *J. Phys. Chem. Ref. Data* **28**, 1453 (1999).
99. B. Eliasson and U. Kogelschatz, *J. Chim. Phys.* **83**, 279 (1986).
100. R. Peyrous, *Ozone Sci. Eng.* **12**, 19 (1990).

101. B. Eliasson and U. Kogelschatz, in *Proc. 8th Int. Symp. on Plasma Chemistry (ISP-8)*, Tokyo (1987), pp. 736–741.
102. U. Kogelschatz and P. Baessler, *Ozone Sci. Eng.* **9**, 195 (1987).
103. V. I. Gibalov, V. G. Samoilovich, and M. Wronski, in *Proc. 7th Int. Symp. on Plasma Chemistry (ISP-7)*, Eindhoven (1985), pp. 401–406.
104. P. J. Crutzen, *Quart. J. R. Met. Soc.* **96**, 320 (1970).
105. H. S. Johnston, *Ann. Rev. Phys. Chem.* **43**, 1 (1992).
106. J. F. Schultz and O. R. Wulf, *J. Am. Chem. Soc.* **62**, 2980 (1940).
107. U. Kogelschatz and B. Eliasson, Ozone Generation and Applications, in *Handbook of Electrostatic Processes* (J. S. Chang, A. J. Kelly, and J. M. Crowley, eds.), Marcel Dekker, New York (1995), Chapter 26, pp. 581–605.
108. U. Kogelschatz, in *Proc. Int. Ozone Symp.*, Basle (1999), pp. 253–265.
109. A. Starke, *Z. Elektrochem.* **29**, 358 (1923).
110. M. Kuzumoto, Y. Tabata, and S. Yagi, *Trans. IEE of Japan* **116A**, 121 (1996) (in Japanese).
111. S. Masuda, K. Akutsu, M. Kuroda, Y. Awatsu, and Y. Shibuya, *IEEE Trans. Ind. Appl.* **24**, 223 (1988).
112. J. A. Wojtowicz, Ozone, in *Kirk–Othmer Encyclopedia of Chemical Technology*, John Wiley & Sons, Inc. (1996), Fourth Edition, Vol. 17, pp. 953–994.
113. J. Hoigné, Cemistry of aqueous ozone and transformation of pollutants by ozonation and advanced oxidation process, in *Handbook of Environmental Chemistry*, (J. Hrubec, ed.), Vol. 5, Part C, Springer, Berlin (1998), pp. 83–141.
114. W. E. Cromwell and T. C. Manley, *Adv. Chem. Ser.* **21**, 304 (1959).
115. E. Inoue and K. Sugino, *Adv. Chem. Ser.* **21**, 313 (1959).
116. B. M. Penetrante and S. E. Schultheis (eds.), *Non-Thermal Plasma Techniques for Pollution Control, Part A: Overview, Fundamentals and Supporting Technologies, Part B: Electron Beam and Electrical Discharge Processing*, NATO ASI Series, Series G: Ecological Sciences, Vol. 34, Springer, Berlin (1993).
117. L. A. Rosocha, G. A. Anderson, L. A. Bechtold, J. J. Coogan, H. G. Heck, M. Kang, W. H. McCulla, R. A. Tennant, and J. P. Wantuck, Treatment of hazardous organic wastes using silent discharge plasmas, in *Non-Thermal Plasma Techniques for Pollution Control* (B. M. Penetrante and S. E. Schultheis, eds.), NATO ASI Series, Vol. G 34, Part B, Springer, Berlin (1993), pp. 281–308.
118. U. Kogelschatz, in *Proc. 8th Int. Conf. on Switching Arc Phenomena/Int. Symp. on Electrical Technologies for Environmental Protection (SAP&ETEP'97)*, Lodz (1997), pp. 299–303.
119. L. A. Rosocha, Processing of hazardous chemicals using silent-discharge plasmas, in *Plasma Science and the Environment* (W. Manheimer, L. E. Sugiyama, and T. H. Stix, eds.), AIP Press, Woodbury, NY (1997), Chap. 11, pp. 261–298.
120. B. M. Penetrante, J. N. Bardsley, and M. C. Hsiao, *Jpn. J. Appl. Phys.* **36**, 7B, 5007 (1997).
121. L. A. Rosocha, *J. Adv. Oxid. Technol.* **4**, 247 (1999).
122. B. M. Penetrante, R. M. Brusasco, B. T. Merrit, and G. E. Vogtlin, *Pure Appl. Chem.* **71**, 1829 (1999).
123. E. M. van Veldhuizen (ed.), *Electrical Discharges for Environmental Purposes: Fundamentals and Applications*, Nova Science Publ., Huntington NY (2000).
124. V. A. Bityurin, M. A. Deminsky, and B. V. Potapkin, Chemical activity of discharges, in *Electrical Discharges for Environmental Purposes: Fundamentals and Applications*, E. M. van Veldhuizen, ed., Nova Science Publ., Huntington, NY (2000), Chapter 4, pp. 49–117.

125. L. A. Rosocha and R. A. Korzekwa, Removal of volatile organic compounds (VOCs) by atmospheric-pressure dielectric-barrier and pulsed-corona electrical discharges, in *Electrical Discharges for Environmental Purposes: Fundamentals and Applications* (E. M. van Veldhuizen, ed.), Nova Science Publ., Huntington, NY (2000), Chapter 10, pp. 245–278.
126. M. Berthelot, *Compt. Rend. Acad. Scé. (Paris)* **82**, 1360 (1876).
127. R. Schwarz and W. Kunzer, *Z. Anorg. Allgem. Chem.* **183**, 287 (1929).
128. I. Traus and H. Suhr, *Plasma Chem. Plasma Process.* **12**, 275 (1992).
129. E. J. Clothiaux, J. A. Koropchak, and R. R. Moore, *Plasma Chem. Plasma Process.* **4**, 15 (1984).
130. M. E. Fraser and R. Sheinson, *Plasma Chem. Plasma Process.* **6**, 27 (1986).
131. I. Sardja and S. K. Dhali, *Appl. Phys. Lett.* **56**, 21 (1989).
132. S. K. Dhali and I. Sardja, *J. Appl. Phys.* **69**, 6319 (1991).
133. M. B. Chang, M. J. Kushner, and M. J. Rood, *Plasma Chem. Plasma Process.* **12**, 565 (1992).
134. W. Sun, B. Pashai, S. K. Dhali, and F. I. Honea, *J. Appl. Phys.* **79**, 3438 (1996).
135. R. H. Zhang, T. Yamamoto, and D. S. Bundy, *IEEE Trans. Ind. Appl.* **32**, 113 (1996).
136. M. B. Chang and T. D. Tseng, *J. Environ. Eng.* **122**, 41 (1996).
137. R. Ruan, W. Han, A. Ning, P. L. Chen, P. R. Goodrich, and R. Zhang, *J. Adv. Oxid. Technol.* **4**, 328 (1999).
138. H. Ma, P. Chen, and R. Ruan, *Plasma Chem. Plasma Process.* **21**, 611 (2001).
139. J. Comes, *Angew. Chem.* **106**, 1900 (1994).
140. A. Ogata, K. Mizuno, S. Kushiyama, and T. Yamamoto, *Plasma Chem. Plasma Process.* **18**, 363 (1998).
141. S. Futamura, A. Zhang, G. Prieto, and T. Yamamoto, *IEEE Trans. Ind. Appl.* **34**, 967 (1998).
142. M. C. Hsiao, B. T. Merrit, B. M. Penetrante, G. E. Vogtlin, P. H. Wallman, R. G. Tonkyn, R. R. Shah, and T. M. Orlando, *J. Adv. Oxid. Technol.* **1**, 79 (1996).
143. A. Ogata, K. Yamanouchi, K. Mizuno, S. Kushiyama, and T. Yamamoto, *Plasma Chem. Plasma Process.* **19**, 383 (1999).
144. A. Ogata, N. Shintani, K. Mizuno, S. Kushiyama, and T. Yamamoto, *IEEE Trans. Ind. Appl.* **35**, 753 (1999).
145. W. C. Neely, E. I. Newhouse, E. J. Clothiaux, and C. A. Gross, Decomposition of complex molecules using silent discharge processing, in *Non-Thermal Plasma Techniques for Pollution Control* (B. M. Penetrante and S. E. Schultheis, eds.), NATO ASI Series, Vol. G 34, Part B, Springer, Berlin (1993), pp. 309–320.
146. A. Sjöberg, T. H. Teich, E. Heinzle, and K. Hungerbühler, *J. Adv. Oxid. Technol.* **4**, 319 (1999).
147. T. Yamamoto, J.-S. Chang, A. A. Berezin, H. Kohno, S. Honda, and A. Shibuya, *J. Adv. Oxid. Technol.* **1**, 67 (1996).
148. G. K. Anderson, H. Snyder, and J. Coogan, *Plasma Chem. Plasma. Process.* **19**, 131 (1999).
149. S. P. Bugaev, V. A. Kushinov, N. S. Sochugov, and P. A. Khryapov, *Plasma Chem. Plasma Process.* **16**, 669 (1996).
150. D. G. Storch and M. J. Kushner, *J. Appl. Phys.* **73**, 51 (1993).
151. H. M. Lee and M. B. Chang, *Plasma Chem. Plasma Process.* **21**, 329 (2001).
152. M. C. Hsiao, B. T. Merrit, B. M. Penetrante, and G. E. Vogtlin, *J. Appl. Phys.* **78**, 3451 (1995).
153. Z. Falkenstein, *J. Adv. Oxid. Technol.* **2**, 223 (1997).
154. R. G. Tonkyn, S. E. Barlow, and T. M. Orlando, *J. Appl. Phys.* **80**, 4877 (1996).

155. T. Yamamoto, K. Mizuno, I. Tamori, A. Ogata, M. Nifuku, M. Michalska, and G. Prieto, *IEEE Trans. Ind. Appl.* **32**, 100 (1996).
156. C. Fitzsimmons, F. Ismail, J. C. Whitehead, and J. J. Wilman, *J. Phys. Chem.* **A104**, 6032 (2000).
157. D. Evans, L. A. Rosocha, G. K. Anderson, J. J. Cogan, and M. J. Kushner, *J. Appl. Phys.* **74**, 5378 (1993).
158. T. Oda, R. Yamashita, T. Takahashi, and S. Masuda, *IEEE Trans. Ind. Appl.* **32**, 227 (1966).
159. S. Futamura and T. Yamamoto, *IEEE Trans. Ind. Appl.* **33**, 447 (1997).
160. A. C. Gentile and M. J. Kushner, *J. Appl. Phys.* **78**, 2977 (1995).
161. H. Snyder and G. K. Anderson, *IEEE Trans. Plasma Sci.* **26**, 1695 (1998).
162. S. J. Yu and M. B. Chang, *Plasma Chem. Plasma Process.* **21**, 311 (2001).
163. R. N. Foster and J. B. Butt, Enhancing reaction rates, US Patent No. 3,674,666 (1972).
164. J.-S. Chang, P. A. Lawless, and T. Yamamoto, *IEEE Trans. Plasma Sci.* **19**, 1152 (1991).
165. C. M. Nunez, G. H. Ramsey, W. H. Ponder, J. H. Abbott, L. E. Mammel, and P. H. Kariher, *Air & Waste* **43**, 242 (1993).
166. T. Yamamoto, P. A. Lawless, M. K. Owen, D. S. Ensor, and C. Boss, Control of volatile organic compounds by a pulsed corona reactor and a packed bed reactor, in *Non-Thermal Plasma Techniques for Pollution Control*, NATO ASI Series, Vol. G 34, Part B (B. M. Penetrante and S. E. Schultheis, eds.), Springer, Berlin (1993), pp. 223–237.
167. M. Kraus, B. Eliasson, U. Kogelschatz, and A. Wokaun, *Phys. Chem. Chem. Phys.* **3**, 294 (2001).
168. M. Higashi, S. Uchida, N. Suzuki, and K. Fujii, *IEEE Trans. Plasma Sci.* **20**, 1 (1992).
169. M. Klein, and R. Seeböck, *Phys. Blätter* **52**, 886 (1996) (in German).
170. B. M. Penetrante, R. M. Brusasco, B. T. Merrit, and G. E. Vogtlin, *Pure Appl. Chem.* **71**, 1829 (1999).
171. B. M. Penetrante, M. C. Hsiao, B. T. Merrit, G. E. Vogtlin, P. H. Wallman, M. Neiger, O. Wolf, T. Hammer, and S. Bröer, *Appl. Phys.* **68**, 3719 (1996).
172. W. O. Niessen, O. Wolf, R. Schruft, and M. Neiger, *J. Phys. D: Appl. Phys.* **31**, 542 (1998).
173. T. Hammer, in *Proc. 7th Int. Symp. on High Pressure Low Temperature Plasma Chemistry (HAKONE VII)*, Greifswald (2000), Vol. 2, 234–241.
174. J. W. Hoard, T. J. Wallington, J. C. Ball, M. D. Hurley, K. Wodzisz, and M. L. Balmer, *Environ. Sci. Technol.* **33**, 3427 (1999).
175. T. Hammer, S. Bröer, and T. Kishimoto, *J. Adv. Oxid. Technol.* **4**, 368 (1999).
176. A. C. Gentile and M. J. Kushner, *J. Appl. Phys.* **78**, 2074 (1995).
177. J. J. Lowke and R. Morrow, *IEEE Trans. Plasma Sci.* **23**, 661 (1995).
178. O. Eichwald, M. Yousfi, A. Hennad, and M. D. Bennabdessadok, *J. Appl. Phys.* **82**, 4781 (1997).
179. Y. S. Mok, S. W. Ham, and I.-S. Nam, *IEEE Trans. Plasma Sci.* **26**, 1566 (1998).
180. R. Dorai and M. J. Kushner, *J. Phys. D: Appl. Phys.* **34**, 574 (2001).
181. L. W. Sieck, J. T. Herron, and D. S. Green, *Plasma Chem. Plasma Process.* **20**, 235 (2000).
182. J. T. Herron and D. S. Green, *Plasma Chem. Plasma Process.* **21**, 459 (2001).
183. J. T. Herron, *Plasma Chem. Plasma Process.* **21**, 581 (2001).
184. R. Dorai and M. J. Kushner, *J. Appl. Phys.* **88**, 3739 (2000).
185. I. Orlandini and U. Riedel, *J. Phys. D: Appl. Phys.* **33**, 2467 (2000).
186. R. Dorai, K. Hassouni, and M. J. Kushner, *J. Appl. Phys.* **88**, 6060 (2000).
187. M. Klein, *Barrierenentladungen zur Entstickung motorischer Abgase*, PhD Thesis, Universität Karlsruhe (1995) (in German).

188. S. Bröer, *Plasmainduzierte Entstickung dieselmotorischer Abgase-Der Einfluss gasförmiger Additive sowie die Kombination mit katalytischen und reaktiven Materialien*, PhD Thesis, Technische Universität München (1997) (in German).
189. R. Dorai, *Modeling of plasma remediation of NO_x using global kinetic models accounting for hydrocarbons*, MS Thesis, University of Illinois at Urbana-Champlaign, 2000, ftp://uigelz.ece.uiuc,.edu/pub/theses/rajesh_ms_thesis.pdf.
190. S. Müller, J. Conrads, and W. Best, in *Proc. 7th Int. Symp. on High Pressure Low Temp. Plasma Chem. (HAKONE VII)*, Greifswald (2000), Vol. 2, pp. 340–344.
191. R. V. de Saint-Auney, *Chimie et Industrie* **29**, 1011 (1933).
192. Yu. N. Zhitnev and Yu. V. Filippov, *Moscow University Chemistry Bull.* **22**, 5 (1967).
193. J. Rutkowsky, H. Drost, and R. Mach, *Beitr. Plasmaphys.* **23**, 181 (1983).
194. D. I. Slovetsky, *Pure Appl. Chem.* **60**, 753 (1988).
195. B. Eliasson, CO_2 Chemistry: An Option for CO_2 Emission Control? in *Carbon Dioxide Chemistry: Environmental Issues* (J. Paul and C.-M. Pradier, eds.), The Royal Soc. Chem., Cambridge (1994), pp. 5–15.
196. S. S. Shepelev, H. D. Gesser, and N. R. Hunter, *Plasma Chem. Plasma Process.* **13**, 479 (1993).
197. K. Okazaki, in *Proc. Int. Symp. on CO_2 Fixation and Efficient Utilization of Energy*, Tokyo, Japan (1993), pp. 37–42.
198. R. Bhatnagar and R. G. Mallinson, Methane conversion in an ac electric discharges at ambient conditions, in *Methane and Alkane Conversion Chemistry* (M. M. Bhasin and D. W. Slocum, eds.), Plenum Press, New York (1995), pp. 249–264.
199. O. Motret, S. Pellerin, M. Nikravech, V. Massereau, and J.-M. Pouvesle, *Plasma Chem. Plasma Process.* **17**, 393 (1997).
200. L.-M. Zhou, B. Xue, U. Kogelschatz, and B. Eliasson, *Plasma Chem. Plasma Process.* **18**, 375 (1998).
201. L. M. Zhou, B. Xue, U. Kogelschatz, and B. Eliasson, *Energy and Fuels* **12**, 1191 (1998).
202. K. V. Kozlov, P. Michel, and H.-E. Wagner, in *Proc. 7th Int. Symp. on High Pressure Low Temp. Plasma Chem. (HAKONE VII)*, Greifswald (2000), Vol. 2, pp. 262–266.
203. B. Eliasson, U. Kogelschatz, B. Xue, and L.-M. Zhou, *Ind. Eng. Chem. Res.* **37**, 3350 (1998).
204. B. Eliasson, C. Liu, and U. Kogelschatz, *Ind. Eng. Chem. Res.* **39**, 1221 (2000).
205. K. Zhang, B. Eliasson, and U. Kogelschatz, *Energy and Fuels* **15**, 395 (2001).
206. U. Kogelschatz, L.-M. Zhou, B. Xue, and B. Eliasson, Production of synthesis gas through plasma-assisted reforming of greenhouse gases, in *Greenhouse Gas Control Technologies* (B. Eliasson, P. F. W. Riemer, and A. Wokaun, eds.), Pergamon, Amsterdam (1999), pp. 385–390.
207. M. Kraus, W. Egli, K. Haffner, B. Eliasson, U. Kogelschatz, and A. Wokaum, *Phys. Chem. Chem. Phys.* **4**, 668 (2002).
208. D. A. Markgraf, *Corona Treatment: An Overview*, http://www.enerconind.com/treating/papers/overview/overview.pdf, (2001).
209. J. L. Linsley Hood, in *Proc. 6th Int. Conf. on Gas Discharges and Their Applications (GD-80)*, Edinburgh (1980), pp. 86–90.
210. T. Uehara, Corona discharge treatment of polymers, in *Adhesion Promotion Techniques: Technological Application* (K. L. Mittal and A. Pizzi, eds.), Marcel Dekker, New York, Basel (1999), Chapter 7, pp. 139–174.
211. K. Pochner, W. Neff, and R. Leber, *Surf. Coat. Technol.* **74/75**, 394 (1995).
212. S. Meiners, J. G. H. Salge, E. Prinz, and F. Förster, *Surf. Coat. Technol.* **98**, 1121 (1998).
213. M. Hudis, Plasma Treatment of Solid Materials, in *Techniques and Applications of Plasma Chemistry* (J. R. Hollahan and A. T. Bell, eds.), John Wiley & Sons, New York (1974), Chapter 3, pp. 113–147.

214. D. Briggs, Applications of XPS in Polymer Technology, in *Practical Surface Analysis by Auger and X-ray Photoelectron Spectroscopy* (D. Briggs and M. P. Seah, eds.), John Wiley & Sons, Chichester (1983), Chapter 9, pp. 359–396.
215. X. J. Dai and L. Kviz, *Study of atmospheric and low pressure plasma modification on the surface properties of synthetic and natural fibres*, Textile Institute 81st World Conf., Melbourne, Australia, April 2001 (www.tft.csiro.au).
216. F. D. Egitto and L. J. Matienzo, *IBM J. Res. Dev.* **38**, 423 (1994).
217. C. M. Chan, T. M. Ko, and H. Hiraoka, *Surf. Sci. Rep.* **24**, 1 (1996).
218. M. R. Wertheimer, L. Martinu, and J. E. Klemberg-Sapieha, Plasma Treatment of polymers to improve adhesion, in *Adhesion Promotion Techniques: Technological Application* (K. L. Mittal and A. Pizzi, eds.), Marcel Dekker, New York, Basel (1999), Chapter 5, pp. 191–204.
219. O. D. Greenwood, R. D. Boyd, J. Hopkins, and J. P. S. Badyal, *J. Adhesion Sci. Technol.* **9**, 311 (1995).
220. J. Salge, *J. de Physique IV* **5**, C5-583 (1995).
221. R. Thyen, A. Weber, and C.-P. Klages, *Surf. Coat. Technol.* **97**, 426 (1997).
222. F. Denes, Z. Q. Hua, W. J. Simonsick, and D. J. Aaserud, *J. Appl. Polymer Sci.* **71**, 1627 (1999).
223. P. Cocolios, F. Coeuret, J.-L. Gelot, A. Villermet, E. Prinz, and F. Förster, *Coating* **32**, 314 (1999).
224. S. P. Bugaev, A. D. Korotaev, K. V. Oskomov, and N. S. Sochugov, *Surf. Coat. Technol.* **96**, 123 (1997).
225. D. Liu, S. Yu, T. Ma, Z. Song, and X. Yang, *Jpn. J. Appl. Phys.* **39**, 3359 (2000).
226. Z. Falkenstein and J. J. Coogan, *J. Appl. Phys.* **82**, 6273 (1997).
227. F. Massines, C. Mayoux, R. Messaoudi, A. Rabehi, and P. Ségur, in *Proc. 10th Int. Conf. on Gas Discharges and Their Applications (GD-92)*, Swansea (1992), pp. 730–733.
228. J. R. Roth, M. Laroussi, and C. Liu, in *Proc. 27th IEEE ICOPS*, Tampa (1992), Paper #P21.
229. P. P. Tsai, L. C. Wadsworth, and J. R. Roth, *Textile Res. J.* **67**, 359 (1997).
230. N. Gherardi, S. Martin, and F. Massines, *J. Phys. D: Appl. Phys.* **33**, L104 (2000).
231. M. Kogoma and S. Okazaki, *J. Phys. D: Appl. Phys.* **27**, 1985 (1994).
232. T. Yokoyama, M. Kogoma, T. Moriwaki, and S. Okazaki, *J. Phys. D: Appl. Phys.* **23**, 1125 (1990).
233. S. Okazaki, S. M. Kogoma, M. Uehara, and Y. Kimura, *J. Phys. D: Appl. Phys.* **26**, 889 (1993).
234. M. Kogoma, S. Okazaki, N. Kanda, H. Uchiyama, and H. Jinno, in *Proc. Jpn. Symp. Plasma Chem.* **4** (1991), pp. 345–350.
235. F. Massines and G. Gouda, *J. Phys. D: Appl. Phys.* **31**, 3411 (1998).
236. F. Massines, R. Messaoudi, and C. Mayoux, *Plasmas and Polymers* **3**, 43 (1998).
237. M. Laroussi, *IEEE Trans. Plasma Sci.* **24**, 1188 (1996).
238. T. C. Montie, K. Kelly-Wintenberg, and J. R. Roth, *IEEE Trans. Plasma Sci.* **28**, 41 (2000).
239. M. Laroussi, I. Alexeff, and W. L. Kang, *IEEE Trans. Plasma Sci.* **28**, 184 (2000).
240. M. Laroussi, G. S. Sayler, B. B. Glascock, B. McCurdy, M. R. Pearce, N. G. Bright, and C. M. Malott, *IEEE Trans. Plasma Sci.* **27**, 34 (1999).
241. S. Yagi, M. Hishii, N. Tabata, H. Nagai, and A. Nagai, *Laser Eng.* **5**, 171 (1977) (in Japanese).
242. M. Tanaka, S. Yagi, and N. Tabata, in *Proc. 8th Int. Conf. on Gas Discharges and Their Applications (GD-85)*, Oxford (1985), pp. 551–554.

243. K. Yasui, M. Kuzumoto, S. Ogawa, M. Tanaka, and S. Yagi, *IEEE J. Quantum Electron.* **25**, 836 (1989).
244. S. Yagi and M. Kuzumoto, *Australian J. Phys.* **48**, 411 (1995).
245. M. Kuzumoto, S. Ogawa, and S. Yagi, *J. Phys. D: Appl. Phys.* **22**, 1835 (1989).
246. S. Wienecke, S. Born, and W. Viöl, *J. Phys. D: Appl. Phys.* **33**, 1282 (2000).
247. B. Gellert and U. Kogelschatz, *Appl. Phys.* **B52**, 14 (1991).
248. Y. Tanaka, *J. Opt. Soc. Am.* **45**, 710 (1955).
249. E. N. Pavlovskaya and A. V. Yakovleva, *Opt. Spectros.* (*USSR*) **54**, 132 (1983).
250. G. A. Volkova, N. N. Krillova, E. N. Pavlovskaya, and A. V. Yakovleva, *J. Appl. Spectrosc.* **41**, 1194 (1984).
251. B. Eliasson and U. Kogelschatz, *Appl. Phys.* **B46**, 299 (1988).
252. A. P. Gochelashvili, A. V. Dem'yanov, J. V. Kochetov, and L. R. Yangurazova, *Laser Phys.* **3**, 140 (1993).
253. V. V. Ivanov, K. S. Klopovskii, Yu. A. Mankelevich, A. T. Rakhimov, T. V. Rakhimova, G. B. Rulev, and V. B. Saenko, *Laser Phys.* **6**, 654 (1996).
254. F. Vollkommer and L. Hitzschke, in *Proc. 8th Int. Symp. on the Science and Technology of Light Sources (LS-8)*, Greifswals (1998), pp. 51–60.
255. A. Oda, H. Sugarawa, Y. Sakai, and H. Akashi, *J. Phys. D: Appl. Phys.* **33**, 1507 (2000).
256. A. M. Boichenko, S. I. Yakovlenko, and V. F. Tarasenko, *Laser and Particle Beams* **18**, 655 (2000).
257. R. J. Carman, B. K. Ward, and R. P. Mildren, in *Proc. 25th Int. Conf. on Phenomena in Ionized Gases (XXV ICPIG)*, Nagoya 2001, Vol. 4, pp. 331–332.
258. U. Kogelschatz, in *Proc. 20th Int. Conf. on Phenomena in Ionized Gases (XX ICPIG)*, Pisa (1991), Invited Papers, pp. 218–227.
259. H. Esrom and U. Kogelschatz, *Appl. Surf. Sci.* **54**, 440 (1992).
260. M. Lenk and R. Mehnert, in *Proc. RadTech Europe*, Basle (2001), pp. 153–158.
261. H. Kumagai and M. Obara, *Appl. Phys. Lett.* **54**, 2619 (1989).
262. H. Kumagai and M. Obara, *Appl. Phys. Lett.* **55**, 1583 (1989).
263. H. Kumagai and K. Toyoda, *Appl. Phys. Lett.* **59**, 2811 (1991).
264. Z. Falkenstein and J. J. Coogan, *J. Phys. D: Appl. Phys.* **30**, 2704 (1997).
265. J.-Y. Zhang and I. W. Boyd, *J. Appl. Phys.* **84**, 1174 (1998).
266. T. Gerber, W. Luethy, and P. Burkhardt, *Opt. Comm.* **35**, 242 (1980).
267. V. M. Borisov, A. M. Davidovskii, and O. B. Kristoforov, *Sov. J. Quantum Electron.* **12**, 1403 (1982).
268. A. M. Boichenko, V. S. Skakun, V. F. Tarasenko, E. A. Fomin, and S. I. Yakovlenko, *Laser Phys.* **4**, 635 (1994).
269. V. F. Tarasenko, M. I. Lomaev, A. N. Pachenko, V. S. Skakun, and E. A. Sosnin, High-power UV excilamps, in *High Power Lasers—Science and Engineering* (R. Kossowsky, M. Jelinek, and R. F. Walter, eds.), Kluwer Academic Publishers, Dordrecht (1996), pp. 331–345.
270. J. Kawanaka, T. Shirai, S. Kubodera, and W. Sasaki, *Proc. SPIE* **3574**, 466 (1998).
271. S. Bollanti, G. Clementi, P. Di Lazzaro, F. Flora, G. Giordano, T. Letardi, F. Muzzi, G. Shina, and Z. E. Zheng, *IEEE Trans. Plasma Sci.* **27**, 211 (1999).
272. A. M. Boichenko, V. S. Skakun, E. A. Sosnin, V. F. Tarasenko, and S. I. Yakovlenko, *Laser Phys.* **10**, 540 (2000).
273. U. Kogelschatz, *Appl. Surf. Sci.* **54**, 410 (1992).
274. K. Stockwald and M. Neiger, *Contrib. Plasma Phys.* **35**, 15 (1995).
275. J.-Y. Zhang and I. W. Boyd, *J. Appl. Phys.* **80**, 633 (1996).
276. I. W. Boyd and J.-Y. Zhang, *Nucl. Instrum. Methods* **B121**, 349 (1997).
277. U. Kogelschatz, H. Esrom, J.-Y. Zhang, and I. W. Boyd, *Appl. Surf. Sci.* **168**, 29 (2000).

278. R. Mehnert, UV Curing Equipment—Monochromatic UV Lamps, in *UV and EB Curing Technology and Equipment* (R. Mehnert, A. Pincus, I. Janorski, R. Stowe, A. Bereika, eds.), John Wiley/SITA (1999), Chapter 4, pp. 83–105.
279. U. Kogelschatz, UV production in dielectric barrier discharges for pollution control, in *Non-Thermal Plasma Techniques for Pollution Control* (B. M. Penetrante and S. E. Schultheis, eds.), NATO ASI Series, Vol. G 34, Part B, Springer, Berlin (1993), pp. 339–354.
280. O. Legrini, E. Oliveros, and A. M. Braun, *Chem. Rev.* **93**, 671 (1993).
281. H. Esrom, J. Demny, and U. Kogelschatz, *Chemtronics* **4**, 202 (1989).
282. J.-Y. Zhang, L.-J. Bie, and I. W. Boyd, *Jpn. J. Appl. Phys.* **37**, L27 (1998).
283. J.-Y. Zhang, B. Lim, and I. W. Boyd, *Thin Solid Films* **336**, 340 (1998).
284. J.-Y. Zhang and I. W. Boyd, *Opt. Mater.* **9**, 251 (1998).
285. J.-Y. Zhang and I. W. Boyd, *Mat. Sci. Semicond. Process.* **3**, 345 (2000).
286. I. W. Boyd and J.-Y. Zhang, *Mat. Res. Soc. Symp.* **617**, J4.1.1. (2000).
287. H. Esrom, J.-Y. Zhang, and U. Kogelschatz, *Mat. Res. Symp. Proc.* **236**, 39 (1992).
288. J.-Y. Zhang, H. Esrom, U. Kogelschatz, and G. Emig, Modification of polymers with UV excimer radiation from lasers and lamps, *J. Adhesion Sci. Technol.* **8**, 1179 (1994).
289. J.-Y. Zhang, H. Esrom, G. Emig, and U. Kogelschatz, Modification of polymers with UV excimer radiation from lasers and lamps, in *Polymer Surface Modification: Relevance to Adhesion* (K. L. Mittal, ed.), VSP International Science Publishers, Utrecht (1996) pp. 153–185.
290. H. Esrom, Y.-J. Zhang, and U. Kogelschatz, Photochemical modification and etching of PTFE with excimer VUV/UV radiation in *Polymer Surfaces and Interfaces: Characterization, Modification and Application* (K. L. Mittal and K.-W. Lee, eds.), VSP International Science Publishers (1997), pp. 27–35.
291. I. W. Boyd, V. Craciun, and A. Kazor, *Jpn. J. Appl. Phys.* **32**, 6141 (1993).
292. V. Craciun, B. Hutton, D. E. Williams, and I. W. Boyd, *Electron. Lett.* **34**, 71 (1998).
293. J.-Y. Zhang and I. W. Boyd, *Appl. Surf. Sci.* **186**, 64 (2002).
294. J. Heitz, H. Niino, and A. Yabe, *Appl. Phys. Lett.* **68**, 2648 (1966).
295. H. Esrom and U. Kogelschatz, *Thin Solid Films* **218**, 231 (1992).
296. C. Beneking, H. Dannert, M. Neiger, V. Schorpp, K. Stockwald, and H. Müller, *Neuartige UV-Lampen auf der Basis stiller Entladungen, BMFT (Bundesministerium für Forschung und Technologie), Forschungsbericht FKZ 12N5695* (1992) (in German).
297. T. Urakabe, S. Harada, T. Saikatsu, and M. Karino, in *Proc. 7th Int. Symp. on the Science and Technology of Light Sources (LS7)*, Kyoto (1995), pp. 159–160.
298. M. Ilmer, R. Lecheler, H. Schweizer, and M. Seibold, in *Proc. SID Int. Symp.*, Long Beach, CA (2000), Digest of Technical Papers, Vol. XXXI, pp. 931–933.
299. S. Mikoshiba, Gas-discharge displays, in *Wiley Encyclopedia of Electrical and Electronic Engineering* (J. G. Webster, ed.), Wiley-Interscience, New York (1999), vol. 8, pp. 233–238.
300. J. K. Lee and J. P. Verboncoeur, Plasma display panel in *Low Temperature Plasma Physics: Fundamental Aspects and Applications* (R. Hippler, S. Pfau, M. Schmidt, and K. H. Schoenbach, eds.), Wiley-VCH: Weinheim (2001), pp. 367–385.
301. H. G. Slottow, *IEEE Trans. Plasma Sci.* **23**, 760 (1976).
302. D. L. Bitzer and H. G. Slottow, in *Proc. 29th AFIPS Conf.*, Washington (1966), pp. 541–547.
303. L. Loeb and J. El Baccal, *J. Appl. Phys.* **33**, 1567 (1962).
304. W. L. Harries and A. von Engel, *Proc. Phys. Soc.* (*London*) **B64**, 916 (1951).
305. H. J. Hoehn and R. A. Martel, *IEEE Trans. Electron. Dev.* **20**, 1078 (1973).
306. I. Revel, Ph. Belenguer, J. P. Boeuf, and L. C. Pitchford, *Pure Appl. Chem.* **71**, 1837 (1999).

307. R. T. Wegh, H. Donker, E. V. D. van Loef, K. D. Oskam, and A. Meijering, *J. Luminesc.* **87–89**, 1017 (2000).
308. M. Miclea, K. Kunze, G. Musa, J. Franzke, and K. Niemax, *Spectrochimica Acta* **B56**, 37 (2001).
309. K. Okazaki and T. Nozaki, Ultrashort pulsed barrier discharges and applications, *Pure Appl. Chem.* **74**, 317 (2002).
310. V. I. Gibalov and G. J. Pietsch, *J. Phys. D: Appl. Phys.* **33**, 2618 (2000).